

Application of stochastic numerical analyses in the assessment of spatially variable unreinforced masonry walls subjected to in-plane shear loading

Lewis J. Gooch^{*}, Mark J. Masia, Mark G. Stewart

Centre for Infrastructure Performance and Reliability, The University of Newcastle, Callaghan, NSW 2308, Australia

ARTICLE INFO

Keywords:

Unreinforced Masonry
Shear Wall
Arched Brick Wall
Piers
Spandrel Beams
Stochastic Finite Element Analysis
Monte Carlo Simulation
Spatial Variability

ABSTRACT

This paper develops a modelling strategy for the finite element analysis of perforated (arched) unreinforced masonry walls subjected to in-plane shear loading. An experimental baseline was used to facilitate an accurate calibration and assessment of the chosen modelling strategy. This study provides the procedure and the results relevant to a stochastic assessment of unreinforced masonry shear walls. These results may be used in future studies of the reliability of these structures and may be applied in the calibration of reliability-based design practices. Utilising a two-dimensional micro-modelling approach, the capacity of a monotonic loading scheme to capture the envelope of a cyclically applied load was examined. It was found that, while the elastic stiffness of the laboratory specimens was overestimated by the finite element models, the peak load and global response was accurately recreated by the monotonically loaded models. Once the applicability of this procedure had been established, a series of spatially variable stochastic finite element analyses were created by considering the stochastic properties of key material parameters. These analyses were able to estimate the mean load resistance of the experimentally tested walls with a greater accuracy than a deterministic model. Furthermore, these analyses produced an accurate estimate of the variability of shear capacity of and the observed damage to the laboratory specimens. Due to the fact that the tested walls failed almost exclusively in a rocking mode, a failure mechanism highly dependent upon the structures' geometry, the variability of the peak strength was minimal. However, the observed damage and presence of some sliding and stepped cracking indicates that the proposed methodology is likely to capture more variable and unstable failure modes in shear walls with a smaller height-to-length ratio or those more highly confined.

1. Introduction

Unreinforced masonry (URM) structures are highly susceptible to damage and collapse when subjected to unfavourable loading conditions. Perhaps the most adverse of these loading conditions is that induced under laterally aligned forces, such as earthquakes or wind events. This vulnerability is due in part to the high mass and initial stiffness of masonry which results in the attraction of higher loading, particularly under earthquake conditions. The effects of this high load attraction are exacerbated by the fact that URM structures have a low tensile resistance and so are at risk of failure and collapse when subjected to high in-plane shear forces, and relatively low out-of-plane loading.

The design of structures intended to resist lateral loading is often concerned with the design and construction of shear walls. These walls are intended to resist any lateral loading through in-plane shear which is

subsequently transferred between storeys and into the structure's foundation. As such, the behaviour, reliability, and method of assessment of masonry shear walls is of key importance in the mitigation of collapse for URM buildings. The application of experimental modelling and finite element analyses (FEAs) allows for researchers to garner a greater understanding of the response of URM walls subjected to in-plane shear loading, and so refine the design procedures and considerations of risk and reliability.

Few studies have considered computational methods for calculating the structural reliability of masonry structures. Early work focused on compression and out-of-plane loading assuming homogenous (non-spatial) material properties (e.g., [5,6,7,38]). Recent developments into the study of URM structures with spatially variable material properties, in conjunction with the application of computational methods of estimating these structures' load resistance, such as in Stewart and Lawrence [35], Lawrence [14], Müller [25] and Li et al., [17,16], have led to

^{*} Corresponding author.

E-mail addresses: lewis.gooch@uon.edu.au (L.J. Gooch), mark.masia@newcastle.edu.au (M.J. Masia), mark.stewart@newcastle.edu.au (M.G. Stewart).

an improved understanding of the structural reliability of these structures. For example, the application of stochastically variable loading and material properties by Stewart and Lawrence [36] resulted in a 66% increase in the compressive design capacity of structural masonry due to the revision of the capacity reduction factor for walls concentrically loaded in compression in the current Australian Standard for masonry design, AS3700 (2018). However, few studies have considered the effect of variable material properties of structures subjected to more complex loading, such as in-plane shear.

The current study expands the work by Howlader et al., [13] by considering the effect of spatially variable and stochastically generated material properties of URM walls subjected to combined gravity and in-plane shear loading. In particular, the current study intends to develop a numerical modelling procedure capable of examining the various failure modes these structural systems are susceptible to; namely, sliding, diagonal shear cracking, rocking and/or toe crushing. Furthermore, through the use of Monte-Carlo simulations, an estimation of the likelihood of each of these failure modes may be made for a given geometric arrangement and loading configuration. Utilising the mean and variability of the failure of these structures will facilitate a reliability analysis in future studies. Such an analysis will allow for the probability of failure given a particular loading mechanism to be examined, and recommendations regarding the conservatism and risk of URM shear walls may be made.

A simplified, two-dimensional micro-modelling approach to masonry modelling, proposed by Lourenço [18], has been used extensively in masonry research [12,9,17,40,13], and has been adopted in the current study using the finite element (FE) software package DIANA 10.3 (2019). This modelling approach allows for the consideration of the nonlinearity of URM structures, with a focus on the response of unit-mortar interfaces [18–19].

2. Description of experimental testing

The current study is based upon the work undertaken by Howlader et al., [13], specifically, the laboratory testing and FE modelling of a series of perforated URM walls. The masonry wall specimens considered in this study are presented in Fig. 1. These walls were subjected to a progressively increasing, cyclic, in-plane shear displacement, up to a peak in-plane drift of 48 mm (2.0%) [13]. The shear load–displacement envelopes of these test specimens were then simulated through the progressive application of a monotonic displacement up to this ultimate displacement. The asymmetric pier tests undertaken in the previous study have been excluded from this paper, and as such the wall configurations considered in this study, with their relevant naming conventions, are as follows where *pre-compression* refers to the average

compression stress in each pier resulting from the constant vertical force applied during testing.

WS_0.2 Shallow spandrel under 0.2 MPa of pre-compression,
 WS_0.5 Shallow spandrel under 0.5 MPa of pre-compression,
 WD_0.2 Deep spandrel under 0.2 MPa of pre-compression, and
 WD_0.5 Deep spandrel under 0.5 MPa of pre-compression.

These specimens, comprised of two wythes, are 230 mm in thickness, utilise common bond coursing and contain a header row of units every fourth course. Furthermore, all of these structures were constructed using solid clay brick units of nominal dimensions: 230 mm long, 110 mm wide and 76 mm high, with 10 mm thick mortar joints and utilising the same mortar mix ratio of 1:2:9 (cement: lime: sand) measured by volume [13].

The application of in-plane lateral loading to the test specimens was undertaken using a horizontally aligned hydraulic jack applied to a steel loading H-beam; a 200UC 46.2, and transferred into the walls via two composite beams bonded to the structure, as shown in Fig. 2. Furthermore, vertical pre-compression was also applied via a hydraulic jack, through a spreader beam and into the composite beams, which were aligned with the piers of the test walls. The results of these experimental wall tests, compared to the FE models produced by Howlader et al., [13],

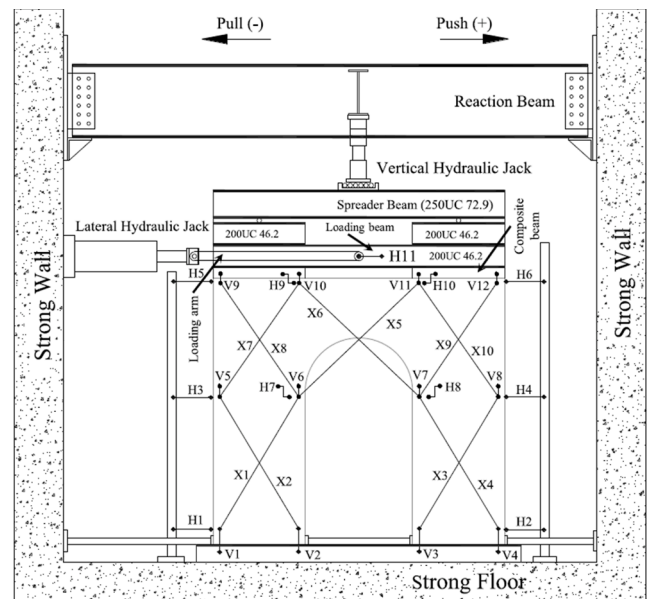


Fig. 2. Elevation of experimental wall test setup and instrumentation [13].

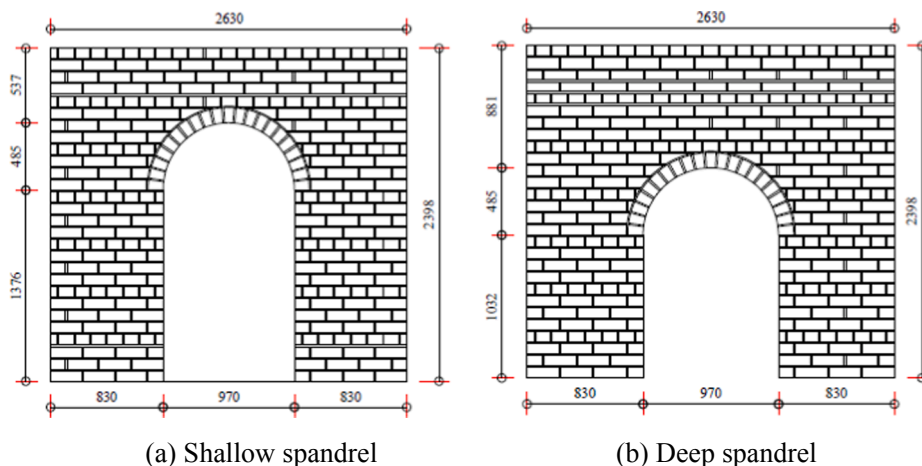


Fig. 1. Wall specimens tested by Howlader et al., [13] (all dimensions are in millimetres).

are shown in Fig. 3.

3. Numerical modelling

The numerical models constructed in the current study represent the full-scale perforated URM walls tested by Howlader et al., [13]. The various geometries and loading configurations are input into the FE software DIANA 10.3, utilising a simplified micro-modelling approach, as outlined in Lourenço [18]. This modelling approach was adopted in the current study as the result presented by Howlader et al., [13] found that a macro-modelling approach, such as is used by Betti et al., [2], over-estimated the peak load resistance of the structures. Furthermore, a detailed micro-modelling approach was not used herein due to the significant increase in computational time; significantly exacerbated by the use of Monte-Carlo simulations.

A similar form of the simplified micro-modelling approach adopted by Howlader et al., [13] was utilised in this study. While there are some distinctions between the modelling strategies used in this study and those used previously; such as the use of higher order elements and a meshing method revised by updates to DIANA, the results produced by the two strategies remain similar, as may be seen in Fig. 4, where (a) the cracking captured using the procedure outlined by Howlader et al., [13], and (b) the cracking modelled using the procedure proposed in this study.

3.1. Model configurations

In the simplified, two-dimensional micro-modelling approach the clay brick units were modelled using eight noded, plane stress elements, CQ16M [3], with a membrane thickness of 230 mm. The simplifying assumption of a membrane thickness, and thus uniform cross-sectional properties, does not allow for an accurate representation of the two wythes interlocked with header rows, however, as only the in-plane behaviour is examined in the current study, this simplification will not

greatly affect the modelled response of the URM walls.

As shown in Fig. 5, the mortar in the masonry structures is not explicitly modelled. In order to represent the geometry of the masonry, each masonry unit is expanded so as to incorporate adjacent bed and perpendicular joints. The interface between the units is then represented with quadratic one-dimensional (CL12I), combined cracking-shearing-crushing interface elements [3], as presented in Fig. 6. These unit-mortar interface elements, along with discrete cracking interface elements [3] used to represent a local failure of masonry units, comprised the FE components capable of capturing the non-linear response of the examined structures.

The quadratic plane stress and line elements used in these models were meshed using a quadratic meshing order. These higher order elements were adopted despite the higher computational expense in order to increase the accuracy of the models. Due to the observed over-estimations of elastic stiffness in masonry FEAs, quadratic elements are preferable as they typically reduce the severity of shear locking, a factor known to stiffen the elastic response of a modelled structure.

Prior to the application of in-plane shear displacements, the vertical pre-compressions noted in Section 2 were applied. These loads were applied in-line with the centreline of the piers, consistent with the experimental testing. Furthermore, due to the relatively low vertical load applied, it was noted that no damage to the spandrel beam was observed during this initial loading phase.

Configuration of appropriate solution algorithm settings was largely determined through trial and error and prior experience with FEAs. A universal configuration was utilised across all FEAs in order to produce consistent results. In this study, a maximum load step of 0.004 (equal to 0.2 mm) was adopted with a cut-off load step value of 1×10^{-8} . Both a force and displacement norm were enforced, each with a tolerance of 0.001; compared to the default norm limits of 0.01 recommended by DIANA. Due to the displacement-based loading applied to each simulation, a displacement-based solver was used as opposed to a force-based or path-following method. This approach was adopted as the models in

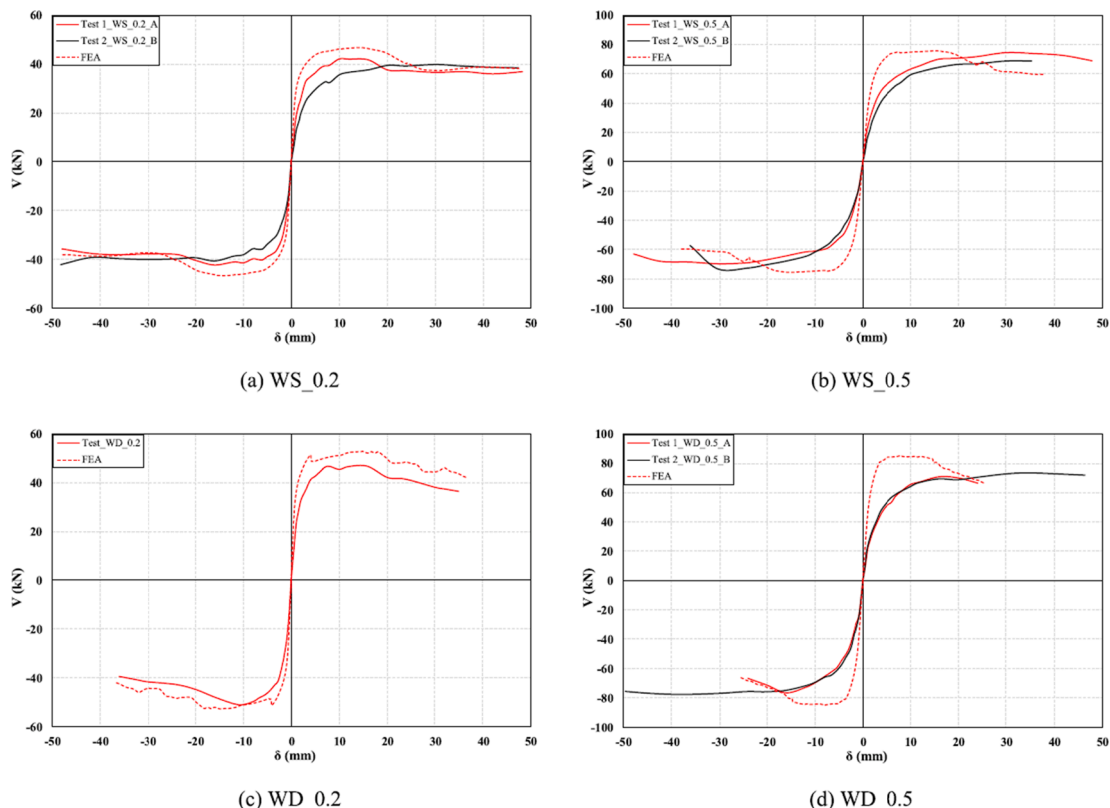


Fig. 3. Load-displacement curves obtained from experimental testings [13].

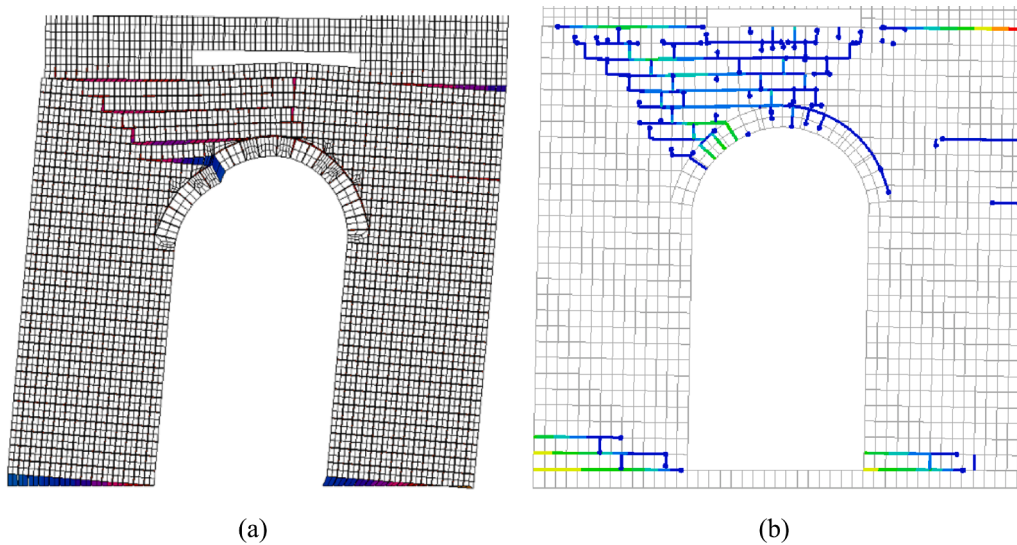


Fig. 4. Comparison of observed and modelled wall crack patterns: (a) FE models by Howlader et al., [13], and (b) Cracking predicted using the proposed modelling strategy.

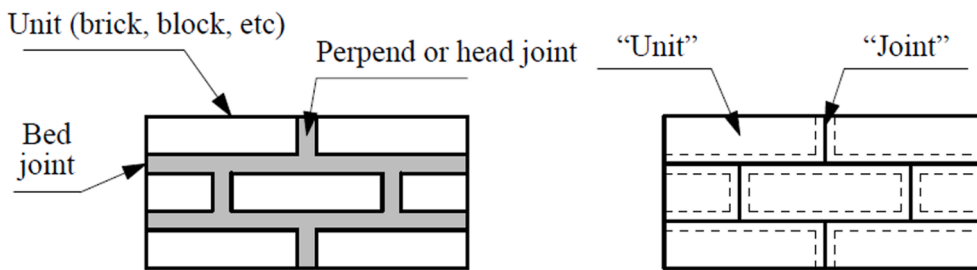


Fig. 5. Expanded geometry of masonry units utilised in the simplified micro-modelling approach [19].

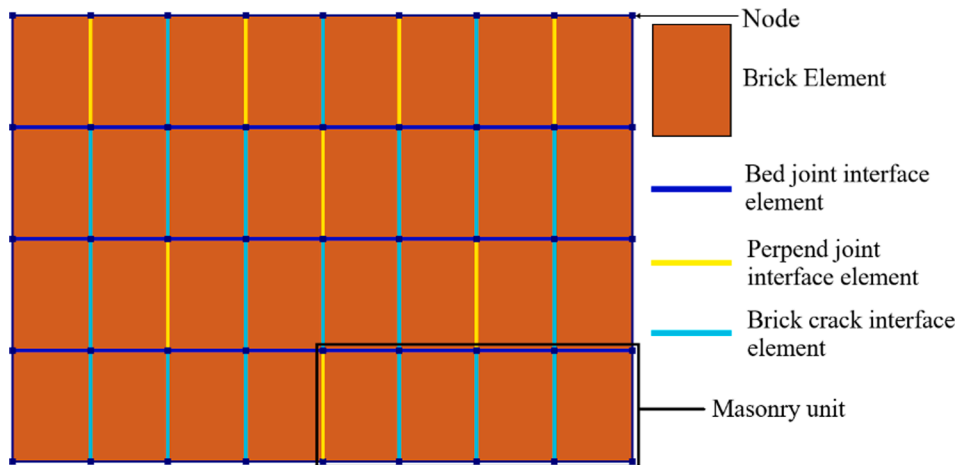


Fig. 6. Simplified micro-modelling approach adopted in the current study.

this study are better suited to a predefined maximum displacement, rather than the maximum load required for a force-based or path-following approach.

During the initial set-up of these simulations, bifurcations of load–displacement behaviour were observed. However, these deviant solution paths were limited to solvers solely using an energy-based convergence norm. It was further observed that the use of an energy-based convergence criteria results in less stable models (i.e.: higher divergence rates), as well as a poorer estimation of the peak strength

relative to the experimental results. Additionally, while numerical noise was observed in the load–displacement response of force- and displacement-based norms, this noise was typically no greater than 3–4% of the peak strength, and did not occur in the linear-elastic phase of the response where bifurcation was most commonly observed.

3.2. Adoption of monotonic loading scheme

A key simplifying assumption made in this study is the adoption of a

monotonic application of loading, as opposed to the application of the cyclic displacement loading scheme adopted in the laboratory testing by Howlader et al., [13]. This simplification was made for several reasons. Firstly, as the focus of this study is to examine the variability of the peak load resistance, it was only necessary to capture the envelope or 'backbone' of the hysteresis loops presented in the previous study. It has been shown in this previous study that the envelope of a cyclic loading scheme may be approximated fairly accurately using a monotonic loading approach. Furthermore, with the obvious alternative to a monotonic loading scheme being the application of the same cyclic loading to an FE model, the applicability of such a model was examined in this study. It was found that these modelling procedures are much more computationally expensive, with model runtimes increasing in some cases by a factor of 50. As this study requires the application of Monte-Carlo simulations, minimising the computational expense of each simulation was essential.

The comparison between the monotonic FEA loading and experimental models is presented in Fig. 7. It may be observed that the monotonically loaded numerical models provide a good estimate of the peak in-plane shear forces measured experimentally. However, these peak resistances are predicted at a significantly smaller in-plane displacement that what was observed experimentally. As discussed above, this is due to numerical models' tendencies to overestimate the elastic stiffness of a structure. As a result, the post-peak softening estimated numerically is more severe that what was observed

experimentally.

Alternatively, the differences in the post-peak behaviour observed between the cyclic laboratory testing and the monotonic numerical modelling may be due to a simplification associated with monotonic loading. During a cyclic loading scheme, there will be an interaction of the shear, traction and compression of elements that have been damaged by previous cycles that will not be present in by monotonically loaded structure. This behaviour may be captured through the application of cyclic loading to an FEA, however as noted above, these analyses are far more computationally expensive and are thus infeasible for the current study.

3.3. Mesh sensitivity analysis

Due to the large number of Monte-Carlo simulations required for a meaningful stochastic finite element analysis (SFEA), the efficiency of the FE models is of particular interest in this study. In order to optimise the mesh density of the FE models, a mesh sensitivity analysis was undertaken to evaluate the variability of the results under different levels of refinement. As an increase in the number of elements directly relates to the time required to construct and evaluate the various models in DIANA 10.3 (2019), the number of elements was minimised.

As can be seen in Fig. 8, refinement of the FE mesh has little effect on the peak load or the overall response of the models. As such, the coarsest mesh that may be permitted using the modelling approach shown in

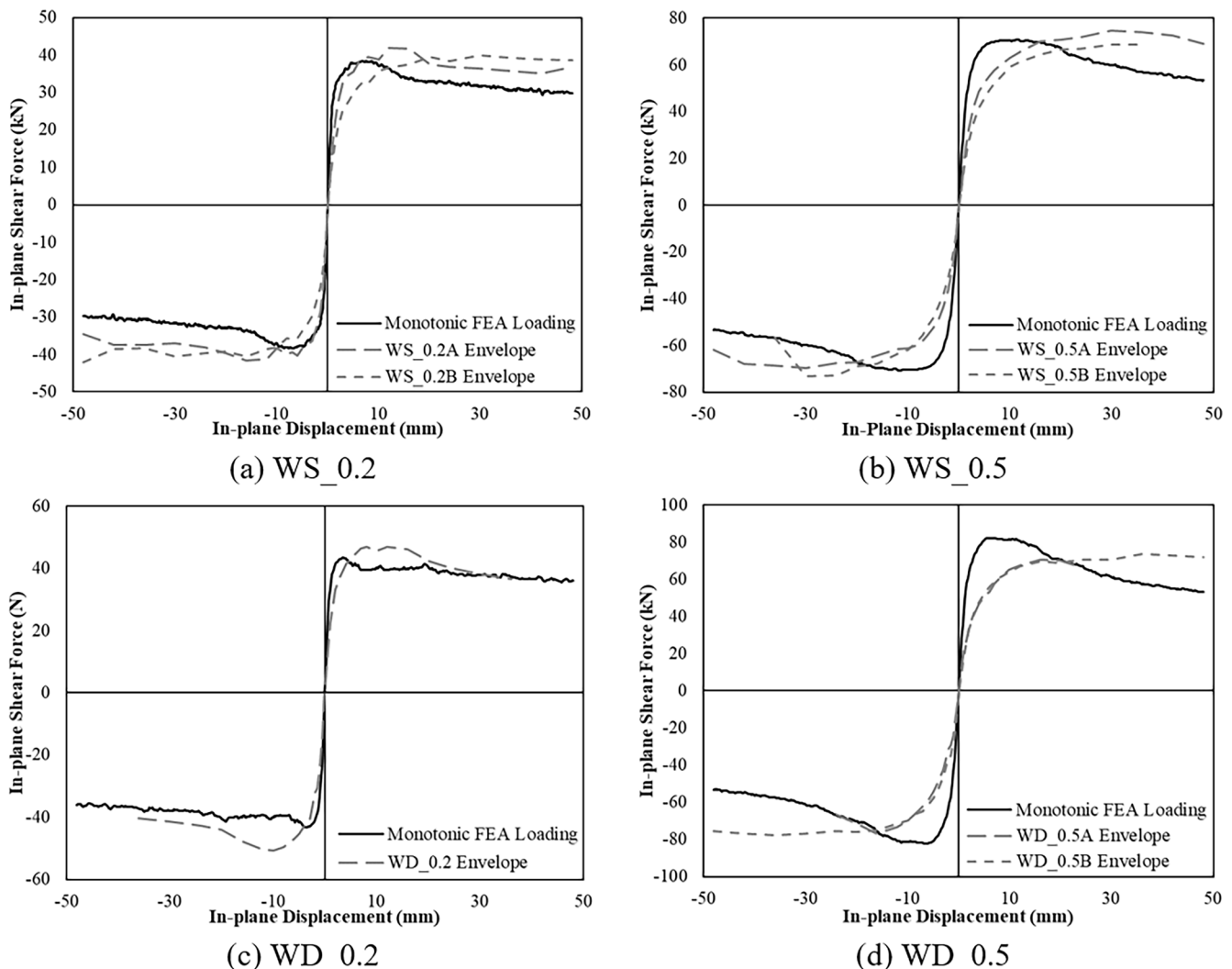


Fig. 7. Comparison of cyclic FEA envelope, monotonic loading response and experimental cyclic tests undertaken by Howlader et al., [13].

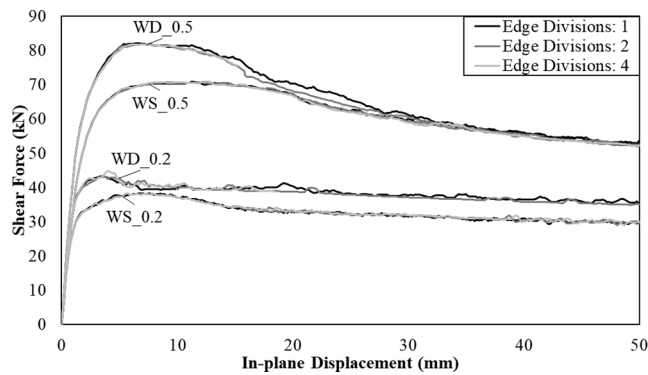


Fig. 8. Effect of mesh density to load-displacement response.

Fig. 6 will be adopted; namely, each masonry unit will be divided into four mesh elements, bounded by bed joints and potential brick cracking interfaces or perpend joints. This adopted mesh density corresponds to a number of edge divisions equal to one (see Fig. 8).

3.4. Material properties

In conjunction with the full-scale laboratory tests, Howlader et al., [13] conducted material characterisation tests using the same type of masonry units and mortar. The masonry prism compression test [4]; Standards [34,33], triplet shear test [8] and bond wrench test (Standards [34,33]) were performed in order to characterise the material properties of the unit-mortar interface. The modulus of rupture test [31] was conducted to define the flexural tensile strength of masonry units. The material properties determined from these laboratory tests have been supplemented by recommended or assumed values which describe those characteristics whose values are considered to not vary significantly; such as the linear elastic properties of steel, or whose values are difficult to accurately determine through the reasonably simple tests performed in the previous study; such as the tensile and shear fracture

Table 1
Deterministic material parameters adopted in FE models.

Material	Property	Value	Unit	Source of data
Brick	Elastic modulus	2502	N/mm ²	[13]
	Poisson ratio	0.2	-	Assumed
	Direct tensile strength	0.71	N/mm ²	[13]
	Tensile fracture energy	0.025	Nmm/mm ²	[18]
Steel Beams	Elastic modulus	200	N/mm ²	(Standards [32])
	Poisson ratio	0.3	-	(Standards [32])
Unit-Mortar Interface	Linear normal stiffness	523	N/mm ³	[13,18,20]
	Linear shear stiffness	218	N/mm ³	[13,18,20]
	Direct tensile strength	0.10	N/mm ²	[13]
	Tensile fracture energy	0.012	Nmm/mm ²	[18]
	Shear bond strength	0.15	N/mm ²	[13]
	Initial friction angle	0.637	Radians	[13]
	Initial dilatancy angle	0.464	Radians	[26]
	Residual friction angle	0.510	Radians	[23]
	Dilatancy suppressing confining stress	-0.75	N/mm ²	[26]
	Shear bond degradation coefficient	1.8	-	[26]
	Masonry compressive strength	7.0	N/mm ²	[13]
	Compressive fracture energy	11.2	Nmm/mm ²	[13]
Shear traction control factor	9.0	-	[18]	
Equivalent plastic relative displacement	0.0128	mm	[13]	
Fracture energy factor (a)	-0.80	mm	[26]	
Fracture energy factor (b)	0.05	Nmm/mm ²	[26]	

energies. The mean values determined from these tests or extracted from the literature, presented in Table 1, form the basis of the deterministic models utilised in the previous and current study.

Several conversions or assumptions have been made of the material properties determined from the laboratory tests for use in the FE models. Firstly, as for both the discrete unit cracking and unit-mortar interface models utilised by DIANA 10.3 (2019), the tensile strength is defined using the direct tensile strength rather than the flexural tensile strengths determined from the modulus of rupture and bond wrench tests. As such, these experimentally determined values have been divided by 1.5 in order to represent this material parameter [13]. The conversion of the modulus of rupture to a direct tensile strength is not prevalent in literature, however, a similar ratio has been used for the flexural and direct tensile strength of plain concrete [29], and has been observed in previous studies of URM structures to produce satisfactory results. For the unit-mortar interface model, this conversion is based upon the findings of Van der Pluijm [39] and Raphael [29].

Furthermore, the determination of shear bond strength and initial friction angle from a shear triplet test may be undertaken by fitting a linear relationship to a plot of shear stress versus normal confining stress; where the zero-confinement intercept describes the shear bond strength and the slope of the line the initial friction coefficient. While this poses little issue for a deterministic model, when the variability of these parameters is of interest, as in this study, the separation of these material properties presents an issue. To resolve this, this study will consider only the variability of the shear bond strength, assuming a constant friction coefficient of 0.74 [13]. The use of a constant initial friction angle is likely a reasonable simplification as this material parameter is typically far less variable than the interface bond strengths and is typically governed by the bonded surfaces; consistent in this study, rather than those factors affecting shear or tensile bond strengths. This simplification allows the shear triplet test data to be converted into a set of shear bond strengths, which have been considered in this study.

It should be noted that, while previous studies of URM structures have considered the effect of a relationship between the tensile strength and tensile fracture energy of both the unit-mortar bond and masonry units, the current study has adopted the constant values shown in Table 1. While it is recognised that the tensile fracture energy of masonry plays a role in the mechanical response of URM structures, such as alternate crack patterns and peak strength estimates, this simplification was adopted so as to be consistent in the deterministic material parameters selected by Howlader et al., [13].

4. Stochastic material models and spatial variability

The parameters of most importance in governing the strength of the walls considered in the current study are, the tensile and shear bond strengths of the unit-mortar interfaces, and the tensile strength of the masonry units. Spatial variability in these parameters will allow for a range of peak strengths to be captured, as critical points in the structure are made weaker or stronger, as well as potentially inducing alternate failure modes; for instance, a lower masonry unit tensile strength in conjunction with a high unit-mortar bond strength may result in a diagonal cracking failure pattern not observed in the deterministic FE models.

In addition to the strength parameters noted above, the stiffness of the interface elements is also of interest, as a high strength bond with a low stiffness may not attract enough load to induce failure until a sufficient amount of cracking and load redistribution has taken place, which may result in a reduction in the peak strength of the structure. In order to examine a variable joint stiffness, the bed and perpend joint thicknesses will also be considered to be spatially variable. While the adopted modelling strategy does not explicitly model the mortar in the structure, the linear normal and shear stiffnesses of these interfaces are inversely proportional to the assumed thickness of the joint [18–19]. However, as the thickness of neither the bed nor perpend joints of the

experimental walls tested have been measured, the stochastic parameters of these thicknesses may be estimated from Mojsilović and Stewart [24]. In this study, the thicknesses of more than 1700 bed and perpend joints were measured across twelve single storey-high walls at three different building sites in Melbourne, Australia and four walls built in a laboratory in Zurich, Switzerland. From the raw data presented by Mojsilović and Stewart [24], the mean and COV of bed and perpend joint thicknesses may be estimated.

The derivation of the adopted probability density functions is discussed in the following sections and is summarised in Table 2.

4.1. Probability distributions

In previous studies of stochastically variable material behaviour, the determination of an appropriate probabilistic distribution has been made through the application of the Kolmogorov-Smirnov (K-S) test, as well as the examination of the goodness-of-fit of the Inverse Cumulative Distribution Function (CDF^{-1}) [12,36–37]. This methodology readily allows for the elimination of unacceptable PDFs, and facilitates adoption of the most suitable distribution to be made by considering the key areas of the CDF; specifically, those whose underestimation or overestimation will have the greatest effect on the accuracy and conservatism of the models.

4.1.1. Mortar joint thickness

In the case of mortar joint thickness, the large sample size results in a rejection of the null hypothesis from the K-S test of each of the examined PDFs, indicating that no distribution is an acceptable fit. However, as this is due to the fact that the maximum allowable deviation calculated from a K-S test is inversely proportional to the number of data points, consideration of the goodness of fit of the CDF^{-1} curves facilitates the selection of a suitable distribution. Unlike the probabilistic distributions that may be considered for a strength parameter, where the lower tail of the CDF^{-1} is typically of the most significance, for the joint stiffnesses of interest to this study, neither tail of the CDF^{-1} produces inherently more conservative results. This is due to the fact that no correlation between stiffness and strength has been assumed, and so the likelihood of attracting load to or from a weak or strong joint may not be readily deduced from the CDF^{-1} plots shown in Figs. 9–13, and thus distributions that most readily fit the 1:1 line are preferable.

In addition to the assessment of the overall goodness of fit of the CDF^{-1} plots, consideration was made to the conservatism, or lack thereof, of any deviations from the 1:1 line. Given that the stiffness of a unit-mortar interface is inversely proportional to the thickness of the mortar joint [3,18,20], PDFs which favour small values of thickness were considered preferable where no significant difference in goodness of fit of two CDF^{-1} s is observed. This was done so as to increase the stiffness of the joints. This would typically result in an increase in the amount of initial load these interfaces would attract and, given low strength of the mortar joints relative to the masonry units, this would result in a more conservative estimate of the peak shear resistance.

Table 2
Stochastic material models adopted for SFEAs.

Property	Mean	COV	Unit	Distribution
Unit modulus of rupture	1.067	23.2%	N/ mm ²	Fig. 11
Flexural tensile bond strength	0.156	31.2%	N/ mm ²	Fig. 12
Shear bond strength	0.149	44.4%	N/ mm ²	Fig. 13
Bed joint thickness	8.87	34.0%	mm	Lognormal
Perpend joint thickness	12.08	29.3%	mm	Lognormal
Ratio of flexural to direct tensile strength of clay brick masonry units	1.53	10.2%	–	Lognormal
Ratio of flexural to direct tensile strength of unit-mortar interface	1.50	13.2%	–	Lognormal

Further to this, while it is typically observed that FE models of masonry structures overestimate the elastic stiffness of experimentally tested structures, as has been observed in this study, a sensitivity analysis revealed that the initial stiffness of the load–displacement curves is largely unaffected by a greater normal and shear interface stiffness. The initial stiffness of the load–displacement curves is far more sensitive to the elastic properties of the masonry unit continuum, and so the conservatism associated with overestimating joint stiffness does not compromise the accuracy of the response curves. It can be seen in Figs. 9 and 10 that the lognormal distribution produces a reasonable, and slightly conservative, estimation of the joint thickness, as well as maintaining a mode smaller than all other distributions. Hence, for both the bed and perpend joints, a lognormal distribution has been adopted.

4.1.2. Interface strength parameters

For material parameters pertaining to strength, the results of experimental testing of these properties are available [13]. As the purpose of this study is to evaluate the application of a stochastic modelling method to recreate experimental wall tests, it was deemed most appropriate to stochastically model the strength values adopted in any stochastic FE models to those obtained also through laboratory testing. Furthermore, given the limited data size for the modulus of rupture, the flexural tensile bond strength and the shear bond strength; these data sets included ten, sixteen, and six data entries respectively, no PDF could be fitted to the data with any reasonable accuracy. This may be observed in the erratic spacing and probability densities shown in the histograms of Figs. 11–13. As such, the modulus of rupture, the flexural tensile bond strength and the shear bond strength were treated as discrete random variables, with each discrete value equating to those measured experimentally.

4.2. Consideration of spatial variability and correlation

A key component of the research presented in this study is the effect of considering spatial variability in the material properties of URM shear walls. While Section 4.1 introduces the stochastic properties that are to be considered, the spatial correlations of these parameters must also be defined. This has been done through the consideration of the physical nature of these correlations, as well as the review of similar relationships in literature. In order to apply spatial variability to each of the SFEAs undertaken in this study, each two-dimensional interface element was prescribed a unique material in DIANA 10.3 (2019). These unique materials were defined as the bed and perpend joints for a given unit, as well as the local unit cracks, and allocated the stochastically generated parameters during the construction of each model.

4.2.1. Correlation of interface strengths

The spatial variability of the chosen stochastic strength properties has been discussed by Heffler [11] and Li [15]. An experimental study by Heffler et al., [12] found that the average adjacent unit correlation coefficient for flexural tensile bond strength was low: between 0.22 and 0.50 for courses within a wall, and recommended a value of 0.4. Li et al., [17] observed that the application of a correlation coefficient of 0.4 to the strengths of adjacent bed joints within a course resulted in a reasonably good agreement between experimental and FE models. The observed correlation of unit-mortar interface strengths occurs due to the fact that bed joint mortar is often laid along the units in the course below such that multiple masonry units may be placed sequentially, and so the characteristics within each run may be similar given their dependence upon the workmanship and mortar properties. However, it is also noted by Heffler et al., [12] that a correlation coefficient of approximately 0.4 represents a fairly weak relationship between variables, and suggests that the spatial correlation of the flexural tensile bond strengths within a course of a wall is not significantly distinct from statistically independent variables [12,14].

Further to this, as the current study considers the tensile and shear

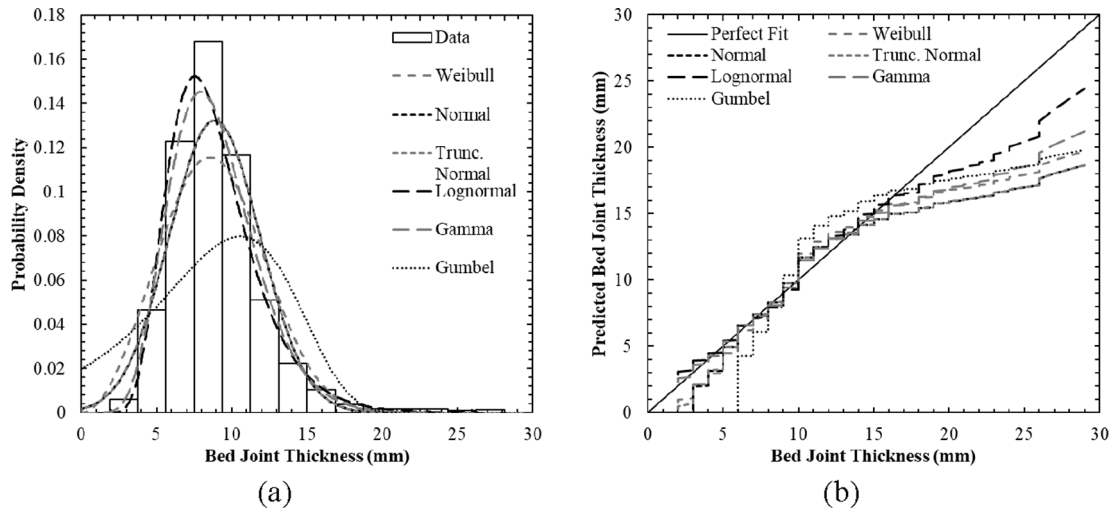


Fig. 9. (a) Probability distributions and (b) Inverse CDF plots of bed joint thickness.

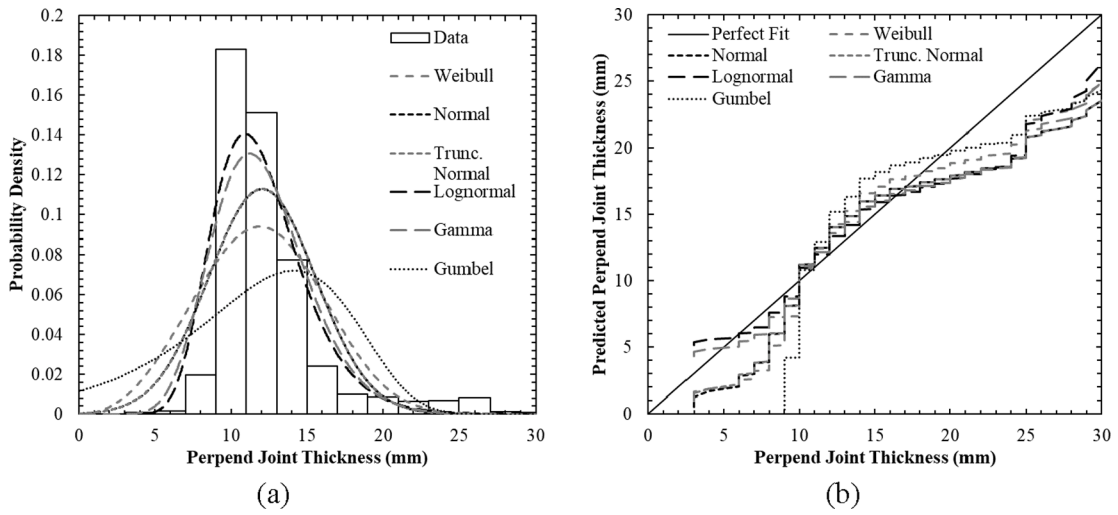


Fig. 10. (a) Probability distributions and (b) Inverse CDF plots of perpendicular joint thickness.

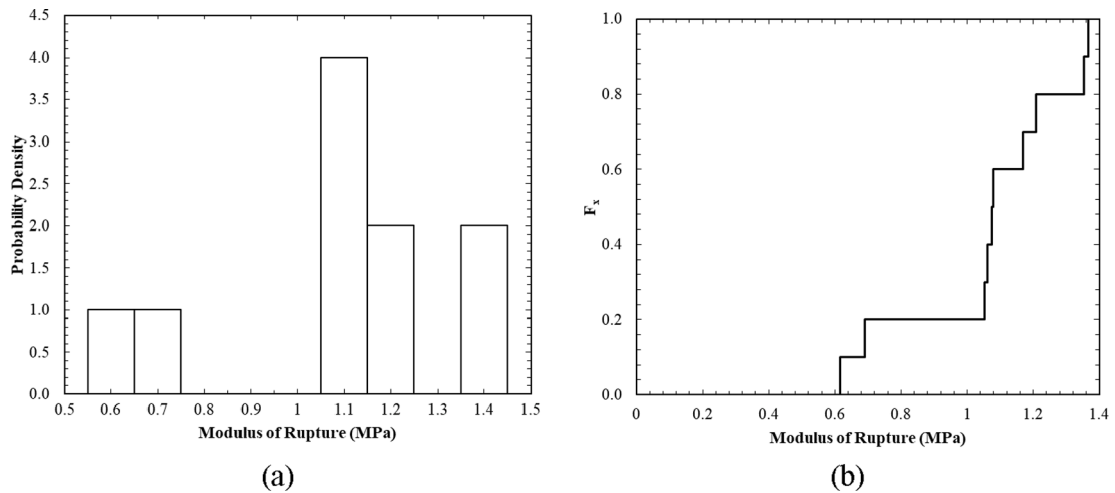


Fig. 11. (a) Histogram and (b) CDF plots of modulus of rupture.

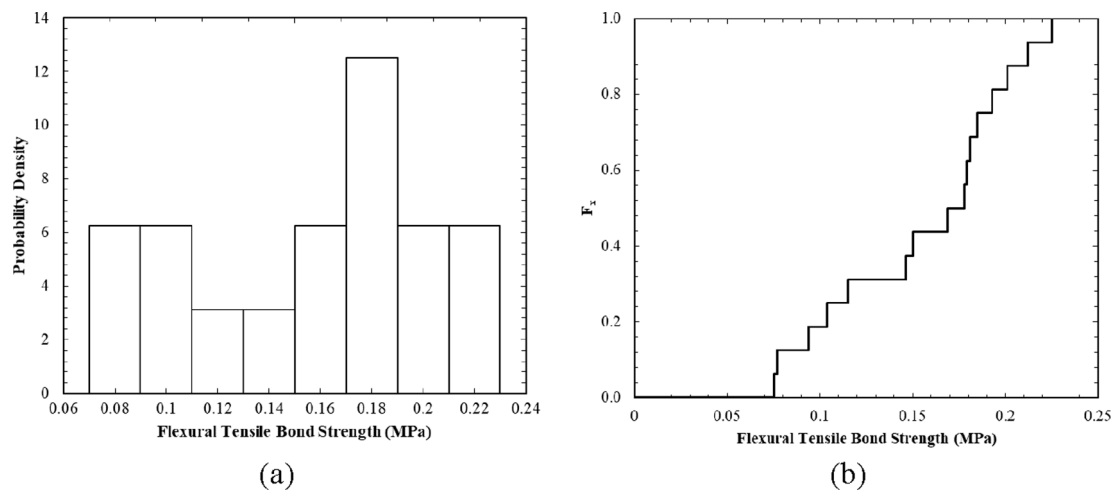


Fig. 12. (a) Histogram and (b) CDF plots of flexural tensile strength.

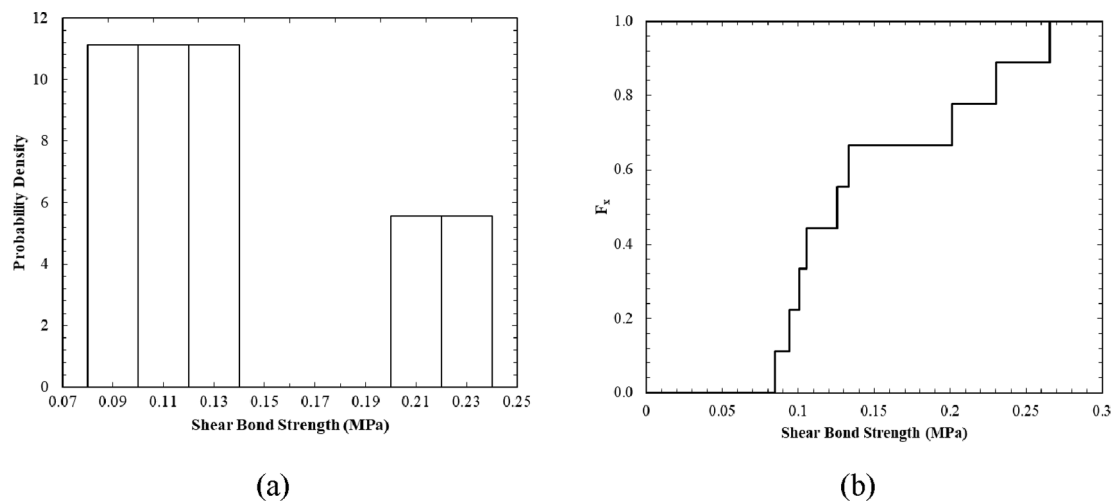


Fig. 13. (a) Histogram and (b) CDF plots of shear bond strength.

bond strengths of the unit–mortar interfaces, as well as the tensile strengths of units, as discrete random variables, rather than being sampled from a continuous PDF, the application of partial correlations is less significant than in the work of Li et al., [17] and Heffler et al., [12]. This diminished significance is due to the fact that the discrete nature of the CDFs of the modulus of rupture, the flexural tensile bond strength and the shear bond strength, will still permit large differences in adjacent material properties for even strongly correlated variables, as well as increasing the likelihood of adjacent interfaces comprising the exact same material properties for weak correlations. As such, for the current study it will be assumed that, within a course, the tensile and shear bond strengths maintain a correlation coefficient of 0; i.e. it will be assumed that these values are statistically independent to those of adjacent units.

Additionally, it is reasonable to assume that the correlation of bond strengths between adjacent perpendicular joints will be less significant than for that of bed joints, as perpendicular joints are placed sequentially as units are installed, and the quality of a given perpendicular joint will have little effect on the quality of subsequent joints. As such, the stochastic generation of perpendicular joint strengths shall also be considered to be statistically independent of adjacent interfaces (i.e. a correlation coefficient, $\rho = 0$).

Finally, as there is no basis to suggest that the properties of any masonry unit affect those of adjacent units as the properties of a masonry unit are dependent upon its manufacture rather than its location within

the wall, the tensile strength of the clay brick masonry units will be assumed to be statistically independent of the strength of adjacent units. However, as it has been assumed that each masonry unit is homogenous across its cross-section, the tensile strength of the three potential cracking interfaces modelled within each masonry unit will be fully correlated, so that the strength of each cracking interface is constant within a single unit.

4.2.2. Correlation of joint thickness

Considering the data presented in Mojsilović and Stewart [24], it was found that the average correlation coefficient for adjacent bed joint thicknesses within a course was approximately 0.13, and 0.10 for perpendicular joints. It is suggested that correlations outside of the limits of $\pm 2\sqrt{1/N}$, are not significantly distinct from statistically independent variables [28,10]. As this limit is approximately ± 0.59 for both the bed and perpendicular joints, this study will assume statistical independence of the thickness of adjacent mortar joints.

Further to this, consideration into the origin of mortar joint variability has been made in order to validate this conclusion. In most practical applications, both in industry and laboratory construction, the thickness of bed joints is indirectly controlled by a level; typically, a string level, placed at the top of the overlying masonry units which ensures that the top of each masonry unit is at the same height. In the case of perpendicular joints, a similar concept is present, where the width of

pend joints is indirectly controlled by the required uniform length of the wall. In both cases, joints may be widened or narrowed in order to accommodate imperfections in the laying of units, as well as irregularities in the heights and lengths of masonry units. As these irregularities in the geometry of masonry units are independent of where in the wall the unit is located, it may be expected that the widening or narrowing of any particular mortar joint is largely independent of those adjacent.

4.2.3. Adopted correlation coefficients

Considering the above, the correlation coefficients, ρ , adopted for the spatial variability of material properties, as well as those representing the correlation of the properties of any single joint are summarised in Table 3.

4.3. Material property conversions and uncertainty

As stated previously, several of the material parameters adopted in the FE models of this study were not directly measured, but rather inferred from laboratory test results. As such, the uncertainty involved in the conversions from flexural to direct tensile strength of the masonry units, as well as that of the unit-mortar interface, has been incorporated into this study's SFEAs in the form of stochastically generated ratios of the measured and adopted material parameters. This allows for the variability between the flexural tensile and direct tensile strengths of both the masonry units and unit-mortar interfaces to be examined.

4.3.1. Flexural to direct tensile strength of masonry units

In order to define the variability of the ratio between the flexural and direct tensile strengths of clay brick masonry units, something that has not been extensively examined in literature, an analogous ratio has been considered in this study and in others [27,17,13]. These studies have all considered a deterministic ratio of flexural to direct tensile strength of 1.5-to-1 for masonry units, similar to the results inferred from Malyszko [22]. This has been based upon a similar relationship derived for plain concrete in AS3600 (2018), based upon the data presented in Raphael [29] from a series of plain concrete cylinder and beam tests.

Considering the relationships between the compressive strength of plain concrete and the corresponding flexural and direct tensile strengths, an estimation of the ratio between the two tensile strengths may be made, as well as its variability. As the data in Raphael [29] does not directly link the two properties, an average of this ratio has been made across 1 MPa increments of the compressive strength, as shown in Fig. 14.

In order to more readily apply the data presented in Fig. 14 to the behaviour of clay brick masonry units, only the data directly applicable to clay brick masonry units should be considered. To this end, an estimate of a ratio between the flexural and direct tensile has been made by considering only those compressive strengths typical of the masonry units utilised by Howlader et al., [13]: specifically, those with a compressive strength of 10 MPa or less. This results in a mean ratio of 1.53-to-1 and is slightly more conservative than that adopted in previous FE studies of masonry [11,26,17,16,13].

Considering the reduced range of data based upon the typical compressive strength of masonry units, a set of PDFs and CDFs⁻¹ were

Table 3
Correlation coefficients adopted in SFEAs.

Correlation of interface properties	Property	Correlation Coefficient
Spatial correlation of units (bricks)	Modulus of rupture	0
Spatial correlation of adjacent mortar joints	Flexural tensile bond strength	0
	Shear bond strength	0
	Bed joint thickness	0
	Mortar joint thickness	0

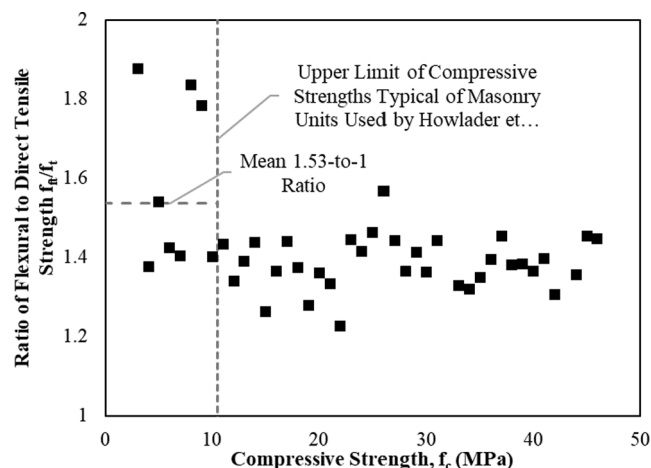


Fig. 14. Observed ratios between flexural and direct tensile strength for plain concrete beams. The upper limit of compressive strengths for masonry units observed by Howlader et al., [13] is noted.

created, and their applicability to the observed ratios of flexural and direct tensile strengths was examined. This was done in the same manner discussed in Section 4.1. It was found that, while none of the examined distributions were rejected by the K-S tests; due largely to the limited number of data points available for compressive strengths less than 10 MPa, none of the selected distributions presented a particularly good fit to the experimental data. In order to overcome this, the fitted distributions were compared to the full range of data presented in Fig. 14. Considering this additional data, it was found that a lognormal distribution presents a very good fit for the lower tail of the CDF¹, as can be seen in Fig. 15. While the underestimation of the upper tail will lead to some non-conservatism for higher values of this ratio, this is a result of the outlying values shown in Fig. 14, and will not overly affect the already low strength of this interface.

In order to determine the variability of the ratio of flexural to direct tensile strength, the effect of variability in testing procedures and specimen variability must be considered. The variability of the model, in this case the ratio of tensile strengths, may then be determined by utilising the following relationship, as presented by Ellingwood et al., [5].

$$V_{Ratio} = \sqrt{V_m^2 - V_{test}^2 - V_{spec}^2} \quad (1)$$

The value of V_m represents the COV determined from the comparison of measured and predicted values. In this case, this would relate to the COV determined from the data presented in Fig. 14. From the truncated data range considered typical of masonry units, a value of V_m of 12.4% has been estimated.

The parameter V_{test} refers to the COV of testing measurements and the parameter V_{spec} refers to the COV of the strengths of the test specimen and control specimens [5]. As per the recommendations in Stewart and Lawrence [37], V_{test} and V_{spec} will be taken to be equal to 0.05. It should be noted that these values of V_{test} and V_{spec} are slightly larger than those of RC beams and columns, whose values typically range from 0.02 to 0.04 [5]. However, as the URM testing procedures relevant to this study, as well as the control specimens themselves, are more difficult to control than in RC testing, a larger value is justified. Furthermore, as a smaller value of say 0.03 for V_{test} and V_{spec} will have a very minor effect on this model; in this case an increase V_{Ratio} by approximately 1.5%, and as there are no literary sources to base this alternate value upon, the value of 0.05, will be maintained. Applying the relationship shown in Equation (1), V_{Ratio} reduced slightly to 10.2% for the conversion of modulus of rupture to direct tensile strength of clay brick masonry units, as summarised in Table 2.

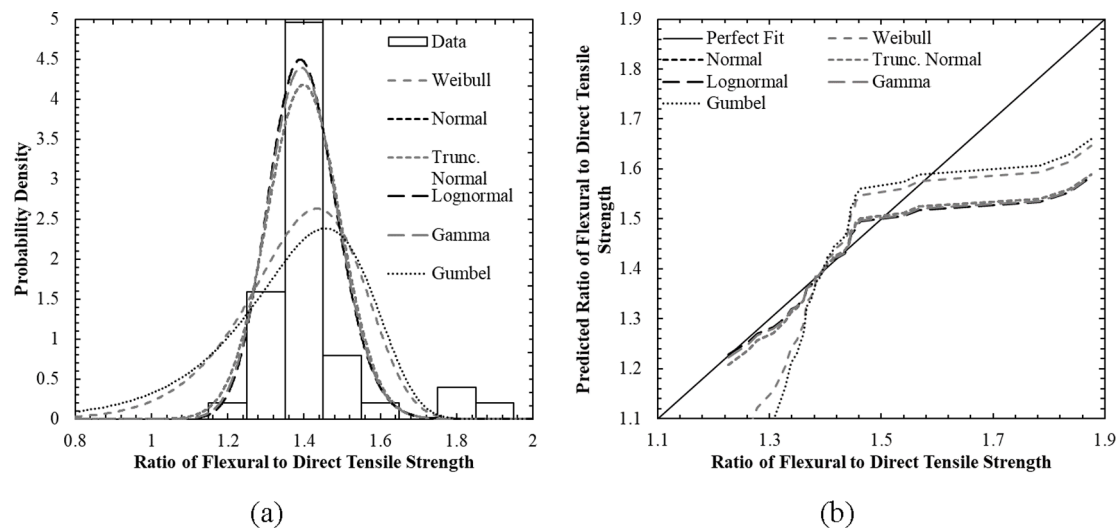


Fig. 15. (a) Probability distributions and (b) Inverse CDF plots of the ratio of flexural to direct tensile strength for all data presented by Raphael [29].

4.3.2. Flexural to direct tensile bond strength of unit-mortar interface

In addition to the model adopted for masonry unit tensile strengths, a similar model is applied to the derivation of the direct tensile strength of the unit-mortar interface. In this case, the flexural tensile strength is derived from a series of bond wrench tests by Howlader et al., [13], and converted to a direct tensile strength by dividing this value by 1.5, as recommended by Van der Pluijm [39]. A similar relationship may be inferred from the experimental data presented by Schmidt, et al. [30].

As in the case of the tensile behaviour of clay brick masonry units, this relationship for the unit-mortar interface has not been extensively researched. It is assumed that a mean ratio of 1.5-to-1 applies between the flexural and direct tensile strength of mortar joints, as has been observed by Van der Pluijm [39]. However, this study does not present a large enough sample of data to produce a meaningful estimation of the variability of this ratio for mortar joints.

As such, the adopted distribution and variability of the model will be assumed from the conclusions made from Raphael's [29] data, as well as the mean value provided by Van der Pluijm [39]. In this case, a lognormal PDF for the ratio of the flexural to direct tensile strength of the unit-mortar interface shall be considered. Furthermore, in order to estimate the COV of this ratio, the COV of 12.4% estimated for masonry units is considered. However, as the discrepancy between the flexural and direct tensile strengths for both masonry units and mortar joints is due to the non-uniformity of tensile strengths across a material's cross-section; something that is perhaps more prevalent and difficult to control in mortar joints, it may be expected that the COV for this ratio is larger for mortar joints than for clay brick units. As such, a slightly larger V_m of 15% has been considered in this study. Finally, the effects of V_{test} and V_{spec} must be considered in the derivation of V_{Ratio} , and as in the previous section, a value of 0.05 has been adopted for both of these parameters. The mean and COV, as well as the adopted PDF of the ratio between the flexural and direct tensile strength of the unit-mortar interface are presented in Table 2.

4.3.3. Tensile and shear bond strength correlation

The final material property relationship that shall be considered in the current study is the relationship between the tensile bond strength and shear bond strength of the unit-mortar interface. It is reasonable to assume that there will be a relationship between these two properties and they both depend upon the quality of the bond between the unit and mortar. AS3700 (2018) recommends a direct relationship between the two properties, providing a constitutive relationship of 1-to-1.25 between the flexural tensile and shear bond strengths of the mortar joints. However, Howlader et al., [13] indicates that, for the experimental walls

under consideration, the mean shear bond strength observed is below this recommendation; with a ratio to the mean flexural tensile bond strength of 1-to-1.

In order to ensure that a reasonable relationship between these properties is enforced in the Monte-Carlo simulations, while not contradicting the observed material behaviours, the two parameters will be assumed to be fully correlated. This will allow the stochastic properties presented in Table 2 to be maintained, while ensuring a high tensile strength results in a high shear bond strength, and vice versa.

5. Deterministic and sfea results

Using the various deterministic and stochastic material properties discussed, as well as the proposed modelling strategy, Monte-Carlo simulations were run for each of the four wall configurations considered in this study. The load versus displacement behaviour was extracted from the results of each simulation, as well as the crack pattern observed at the point of peak resistance and at the ultimate or collapse displacement. From these results, the mean and COV of the peak in-plane shear force was determined for each of the examined walls, and investigation into the observed cracking patterns, non-linear response and the failure mechanism of each simulation could be determined. Furthermore, by considering the bilinearisation method proposed by Magenes et al., [21], an estimation of the ductility factor, μ , has been made.

5.1. Peak in-plane shear force

Prior to the commencement of any Monte-Carlo simulations, the suitability of the FE modelling strategy proposed in this study was examined through the application of deterministic FE models. A comparison of the estimated peak load resistance derived in this study and that of Howlader et al., [13] is summarised in Table 4.

It was found that in three out of the four wall configurations, the observed difference between the experimental and FE models was reduced through the application of the modelling strategy proposed in this study. It should also be noted that while a greater difference was observed in the case of WD_0.2, this wall configuration maintains the smallest number of experimental tests; only a single test and thus two values for the peak load, and so this discrepancy may be attributed to the greater uncertainty in the estimated experimental mean. Furthermore, it is noted that in all cases, the proposed modelling method yields more conservative estimates of the experimental mean than in the previously proposed methodology [13].

Table 4
Comparison of proposed modelling strategy to experimental and FE models presented in previous study.

Wall configuration	Experiment sample size	Experiment mean (kN)	Howlader et al., [13]	Current study
			Deterministic FEA peak load (kN)*	Deterministic FEA peak load (kN)*
WS_0.2	4	41.3	46.6 (12.8%)	39.5 (4.4%)
WS_0.5	4	71.5	75.6 (5.7%)	70.8 (1.0%)
WD_0.2	2	48.7	52.8 (8.4%)	43.4 (10.9%)
WD_0.5	4	74.6	85.2 (14.2%)	82.2 (10.2%)

* Bracketed values refer to percentage difference from experimental mean.

After the validation of the deterministic modelling scheme, the stochastic material models discussed previously were implemented in four sets of Monte-Carlo simulations. The results of these simulations, as well as their convergence, are discussed in the following sections.

5.1.1. Monte-Carlo convergence

An important issue to address during the implementation of Monte-Carlo simulations is the definition of the minimum number of simulations required to reasonably capture the behaviour and the failure modes of the examined walls. This was done in several ways, firstly, the behaviour of each simulation was examined so that an understanding of the individual likelihoods of potential failure modes could be estimated and the number of simulations adjusted so as to garner a suitable approximation of the probabilities of each of these occurrences. It was found that a rocking failure was almost exclusively observed.

Given the inherent stability of the results observed, a quantitative method of determining the suitability of the number of simulations was utilised. This was done by the estimation of the 95% confidence limits of the sample means shown in Table 5. These confidence limits are more readily interpreted as normalised confidence errors; specifically, the distance to the 95% confidence limits from the mean, normalised by the mean of each configuration.

It was observed that for all four cases, this confidence error was very small for 250 simulation runs: less than 0.4% of the mean. This is largely due to the small COV estimated for each of the wall configurations and indicates that, so long as no alternate failure modes; which would result in notable outliers, are excluded, the relatively small number of simulations undertaken in this study still produces a good estimate of the peak in-plane load resistance. This conclusion resulted in a reduction in the number of simulations run for WD_0.2 and WD_0.5 to 100 simulations from the 250 simulations undertaken for WS_0.2 and WS_0.5. The suitability of the number of simulations adopted in this study was also examined through the creation of convergence diagrams, such as those shown in Fig. 16. It may be observed that the mean and COV converge to a stable value quite quickly.

In the event that a simulation diverged prior to the formation of a clear peak strength, further investigations were made. This included revisions to solution algorithm settings in order to make the analysis more robust. This allowed for conclusions to be drawn regarding whether or not the divergence has occurred due to an early and unstable collapse of the simulated structure or if it were simply a divergent

configuration and could be excluded from the analysis. As a suitably robust solver was created prior to the commencement of any Monte-Carlo simulations, this methodology was only applied to eight simulations for the WS_0.5 configuration. It was found that each of these cases were numerically unstable and thus were excluded from further analysis.

5.1.2. SFEA results

Once convergence of the SFEA results was established, meaningful results could be extracted from the Monte-Carlo simulations. Scattergrams of each of the four sets of simulations are shown in Fig. 17. Furthermore, the four dashed lines shown in Fig. 17 represent the peak load estimated from the positive and negative loading directions in the experimental tests undertaken by Howlader et al., [13], while the dotted lines indicate the peak load estimated from the deterministic FE models.

The deterministic estimate of peak load resistance is expected to be close to the mean value determined from a set of SFEAs, however, there is a notable outlier observed in Fig. 17. In the case WD_0.5, the deterministic model represents the upper 97th percentile of peak shear force estimated. The reason for this discrepancy is due to a variation in the post-cracking, pre-peak response of the structure; the inclusion of bed joints with a lower than average shear bond strength in the deep spandrel of the structure has resulted in more adverse cracking of this region. The presence of a weaker than average shear bond strength in the spandrel of these structures is common across all SFEAs: there are 137 distinct bed joint interfaces in the spandrel, so the likelihood of encountering a below average strength interface is extremely high.

While this distinction does not significantly change the overall response of the structure, with a common residual strength and load–displacement curve shape, this more adverse cracking pattern results in a premature post-cracking softening of the structure, causing the peak load to be reduced by 2 kN on average, relative to that value obtained from the deterministic model. The significance of this deviation is compounded by the low inherent variability of the observed failure mechanism of WD_0.5. With a COV of peak strength estimated at 1.5%, a deviation of only 2 kN is significant.

The results of the SFEAs are summarised in Table 5. It was observed that the mean peak load estimated from the Monte-Carlo simulations provided a better representation of the experimentally tested walls than the initial deterministic models. The reduction in the difference between the experimental mean peak load using the SFEA method proposed in this study compared with the analysed deterministic models, ranges from 41% for WS_0.2 to 26% for WD_0.5.

While the results of SFEAs indicate that the examined specimens maintain a very low variability, this does not contradict what was observed in the experimental testing of these structures. In both cases, a small COV has been estimated for each wall configuration, the largest being 5.6% in the case of the experimental testing of WD_0.2; it is also noted that the estimation of this COV may be inaccurate as it is based upon only two values, and so may change if supplemented by additional tests. This apparent stability of strength is likely caused by the geometric configuration of the structures resulting exclusively in a rocking failure mode, an inherently invariable failure mechanism. Furthermore, while it may be observed that the COV of the SFEAs peak load is significantly different from that of the laboratory specimens, with the largest

Table 5
Experimental and FEA approximations of the mean and variability of the peak load resistance.

Wall configuration	Mean			COV	
	Experimental (kN)	SFEA (kN)*	Deterministic (kN)*	Experimental	SFEA
WS_0.2	41.3	39.6 (4.1%)	39.5 (4.4%)	2.4%	2.0%
WS_0.5	71.5	71.0 (1.0%)	70.8 (1.0%)	3.9%	1.2%
WD_0.2	48.7	45.0 (7.6%)	43.4 (10.9%)	5.6%	2.0%
WD_0.5	74.6	80.2 (7.5%)	82.2 (10.2%)	4.3%	1.4%

* Bracketed values refer to percentage difference from experimental mean.

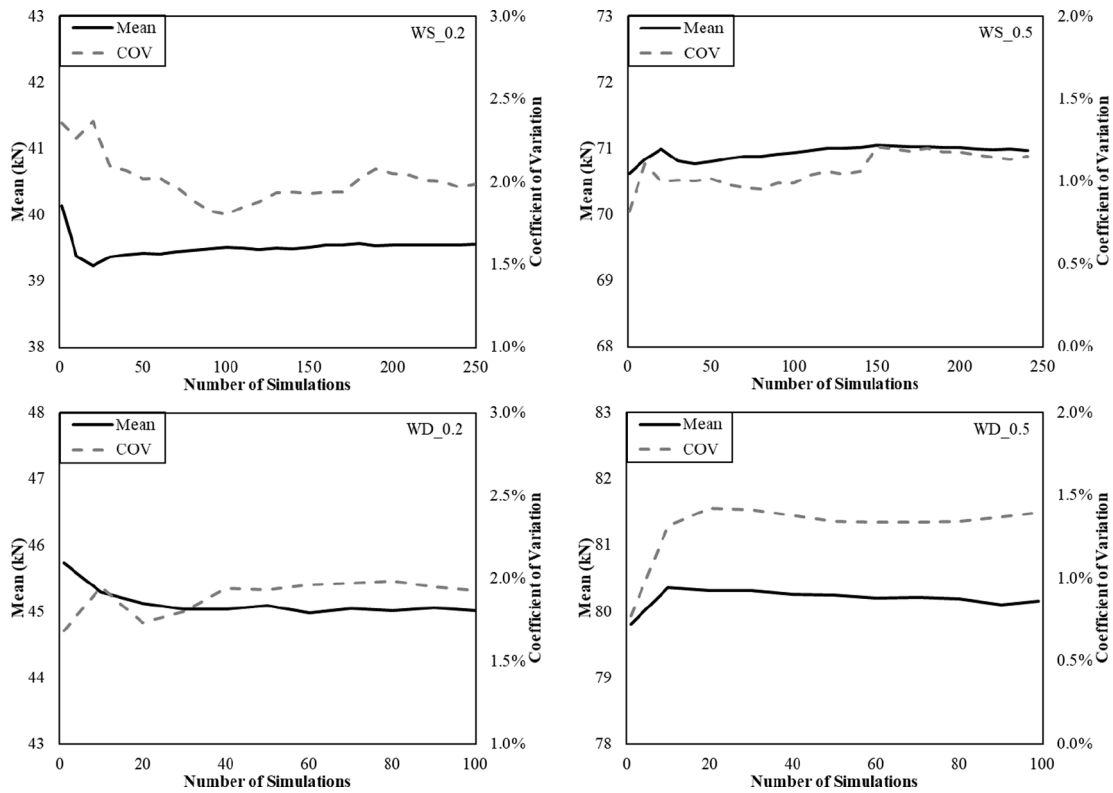


Fig. 16. Convergence diagrams of the mean and COV of each wall configuration.

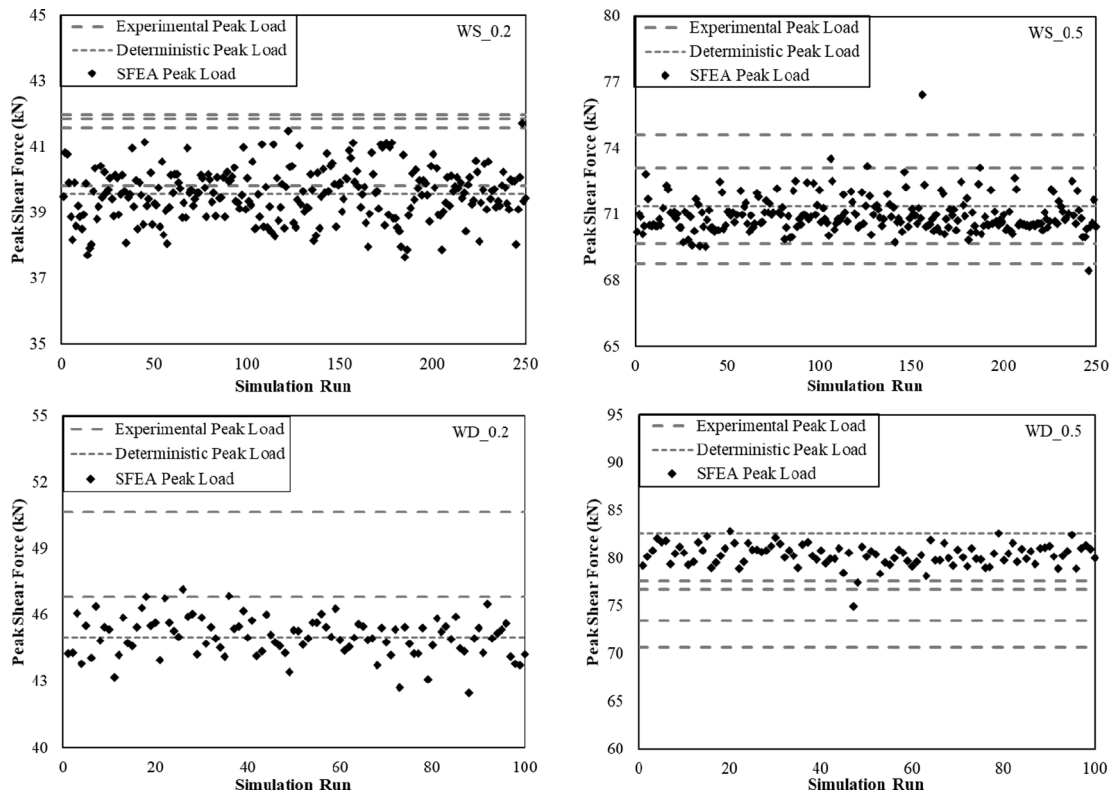


Fig. 17. Peak shear forces obtained from SFEAs compared to the load resistances obtained from experimental testing.

difference being a reduction of more than 50%. However, the COVs for the experimental specimens shown in Table 5 do not consider the effect of variations in the testing procedure (V_{test}) nor the variation in

specimens themselves (V_{spec}), and consideration of these values would result in a significant reduction in the COV of the experimental peak load.

Due to the low variability of the experimental results, appropriate values for V_{test} and V_{spec} are difficult to assume. The proposed value of 0.05 adopted for the material testing undertaken by Howlader et al., [13] is not appropriate in this case, as such values would cause a non-result when applied in Equation (1). Consideration of the lower bound values of 0.04 and 0.02 proposed by Ellingwood et al., [5] for RC beams and columns would still cause this issue in three of the four experimental testing configurations. As the variations in the testing measurements and the experimental specimens were not measured, accurate estimations of their values, and subsequent correction of the variability of the experimental peak load, cannot be made in this study.

As discussed previously, URM walls subjected to in-plane shear loading can fail in four distinct manners: shear sliding, diagonal cracking, rocking, and toe-crushing. The manner of failure is dependent upon the material properties and confining pressure, but also upon the geometry of the structure. Walls with a large height-to-length ratio, such as the pier elements of the specimens examined in this study, typically fail due to rocking or, if the confining stress is great enough, toe-crushing. As such, it is not unexpected that almost all the Monte-Carlo and experimental simulations captured a peak load failure mechanism of heel cracking and rocking of the piers. Furthermore, given the low strength of the unit-mortar tensile bond strength, as well as the potential for cracking to initiate readily in any of the first few courses of the walls; as shown in Section 5.2, it is not unexpected that such a low variability has been observed. It would be expected that as the height-to-length

ratio was reduced, alternate failure modes would begin to become apparent in the Monte-Carlo simulations, resulting in different load–displacement behaviour.

5.2. Cracking patterns

In addition to the peak strength and variability of such, the peak and post-peak cracking in each of the Monte-Carlo simulations and how it compares to what has been observed experimentally is significant in this study. The damage that occurs within URM walls when subjected to in-plane shear loading is perhaps the best indicator of the failure mechanism of the structure, and in the case of SFEAs, this provides another tool in determining the likelihood and variability of distinct failure modes.

The cracking patterns observed at both the point of the peak load and at the ultimate/collapse displacements were examined in this study. As discussed above, it was observed that all of the FE models exhibited a rocking failure, with cracking typically initiating in the first to third bed joints of the tensile pier. Furthermore, it was also typically observed that an increased confining stress resulted in an increase in spandrel damage, as well as the amount of stepped cracking observed in the piers; typically, the compression pier, while an increased spandrel depth reduced the spandrel damage at smaller displacements, but had little effect on the cracking predicted in the piers. These trends are highlighted in Figs. 18 and 19. It should be noted that the models shown in Fig. 18 are the same simulation as in Fig. 19 represented at a different load step, and

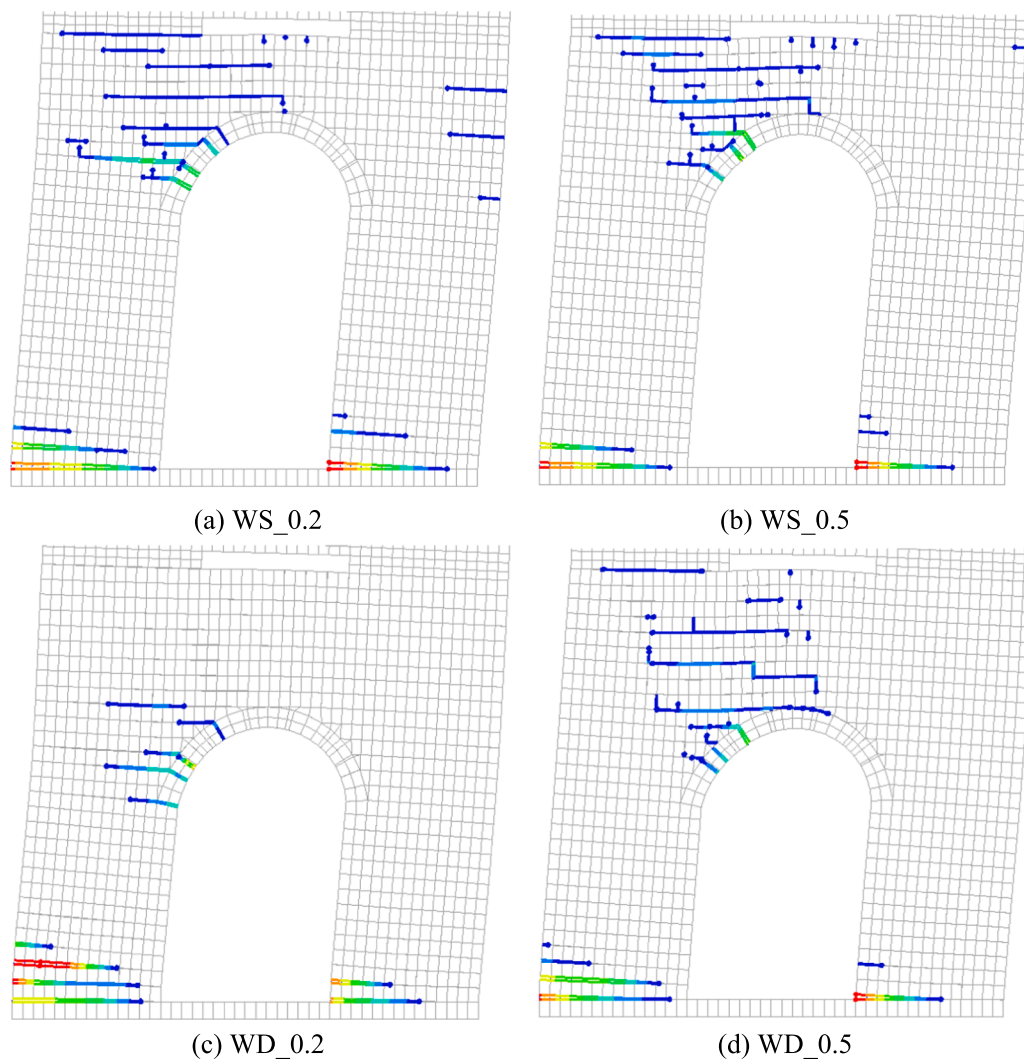


Fig. 18. Typically predicted cracking at point of peak load resistance.

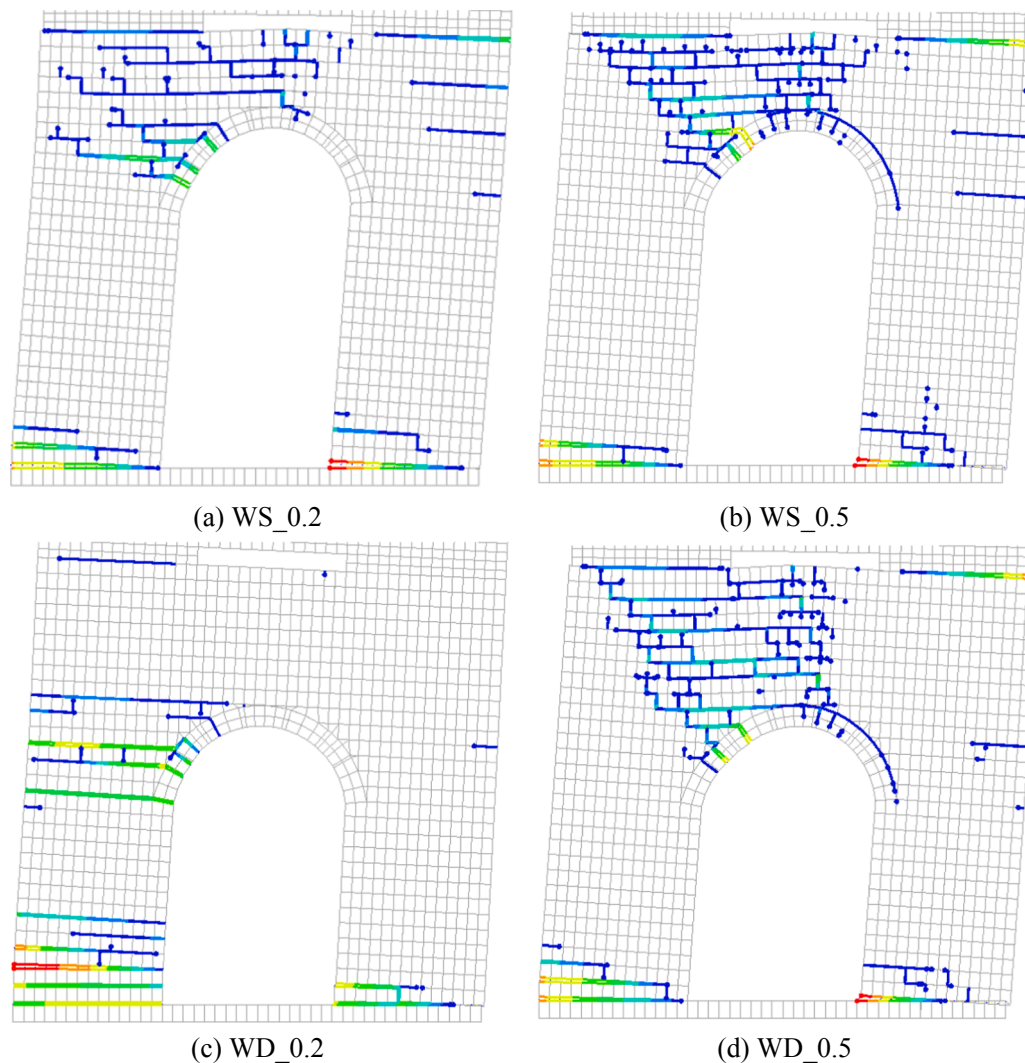


Fig. 19. Typically predicted cracking at ultimate/collapse displacement.

as such show the typical progression of cracking within each configuration.

The crack patterns observed in these SFEAs are a good representation of the observed experimental damage. While the structures examined in this study are not governed by sliding or diagonal cracking failure mechanisms, the damage captured by the proposed modelling strategy indicate that such modes may be examined in future studies. Furthermore, the damage observed in these FE models indicate that the cracking induced by cyclic loading can be readily captured by a monotonic loading scheme.

5.3. Ductility

In order to estimate the ductility of each of the wall configurations, the bilinearisation method proposed by Magenes et al., [21] was adopted. This method was utilised as it is well suited to a stiff elastic response, as opposed to the method proposed by E2126-11 [1]. This is due to the initial assumption regarding the cracking load of the structure. In the case of the method given by Magenes et al., [21], the initial cracking load is assumed as 70% of the peak load resistance recorded in the test, while the procedure outlined in E2126-11 recommends this value as 40% of the peak [1].

5.3.1. Force-displacement response

A key limitation of any estimates of ductility made from the proposed

FE modelling strategy is the overestimation of the initial elastic response of the URM walls. As can be seen in Fig. 20, this linear-elastic region is typically markedly stiffer than what is observed in the experimental tests. As a result, the peak load resistance (and yield displacement in the bilinearised response) is achieved at a much smaller displacement, and so the true ductility of the structure is likely to be overestimated.

While the numerically predicted post-peak responses shown in Fig. 20 show significantly greater softening within the range of displacements examined in this study, it is likely that a similar degree of softening may occur experimentally at a larger in-plane displacement; this is indicated in several of the experimental envelopes whose load-displacement curves begin to decrease more rapidly once the peak strength has been achieved. Conversely, if the overestimated elastic stiffness of the numerical models could be corrected, it may be expected that similar force-displacement behaviours may be captured for higher in-plane displacements. Correction of this behaviour would likely take the form of a stiffness factor applied to the linear normal and shear stiffnesses of the masonry unit continuum elements.

5.3.2. Ductility factors

As noted above, the underestimation of the yield displacement results in an overestimation of the ductility estimation for each of the numerically analysed structures. This is due to the ductility factor being inversely proportional to the yield displacement. While this non-conservatism is somewhat countermanded by the fact that a much

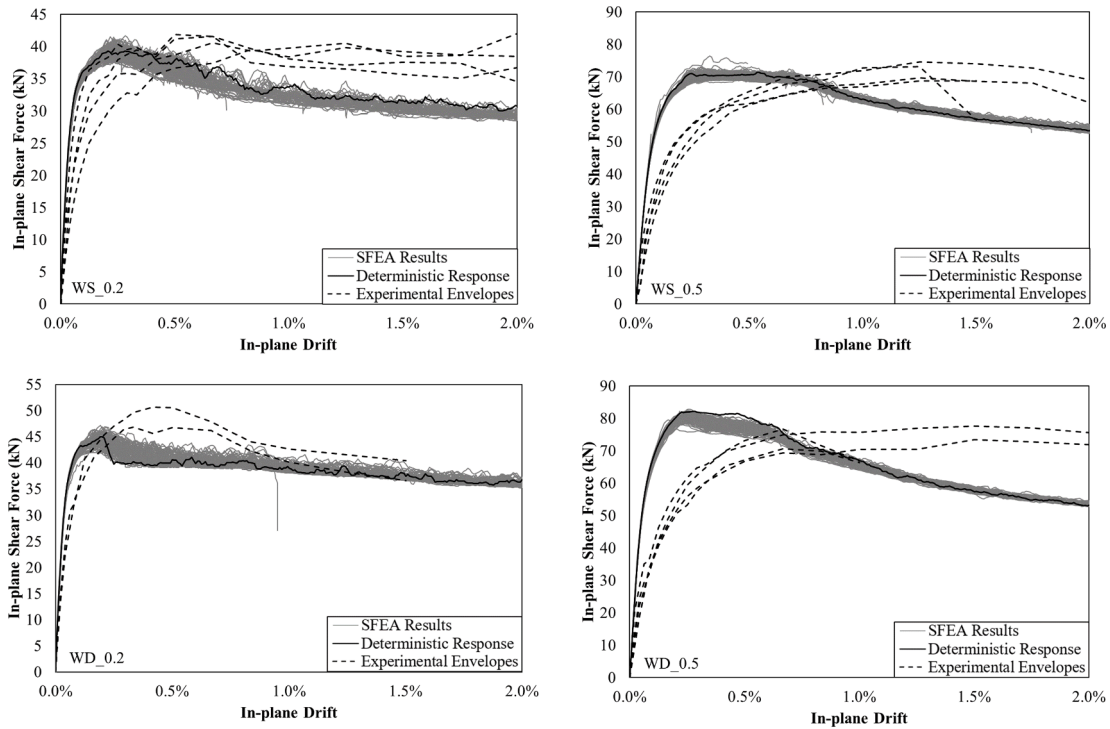


Fig. 20. Comparison of force–displacement responses of SFEA simulations, deterministic FE models and experimental hysteresis envelopes.

larger degree of post-peak softening is observed when the elastic stiffness is overestimated, this may result in an underestimation of the ultimate displacement, which is typically defined at the point at which the post peak load resistance has fallen below 80% of the peak value [21,1]. However, in the cases examined in this study, a post peak load reduction of more than 20% was rarely achieved within the drift displacements

considered, and so a non-conservative estimate of the ductility is likely to have been made. This can be seen in Fig. 21, with the notable exception being WS_0.2, where the scattergrams represent each of the four sets of SFEAs, the dashed lines represent the results estimated from the experimental tests undertaken by Howlader et al., [13], and the dotted lines indicate those obtained from the deterministic FE models.

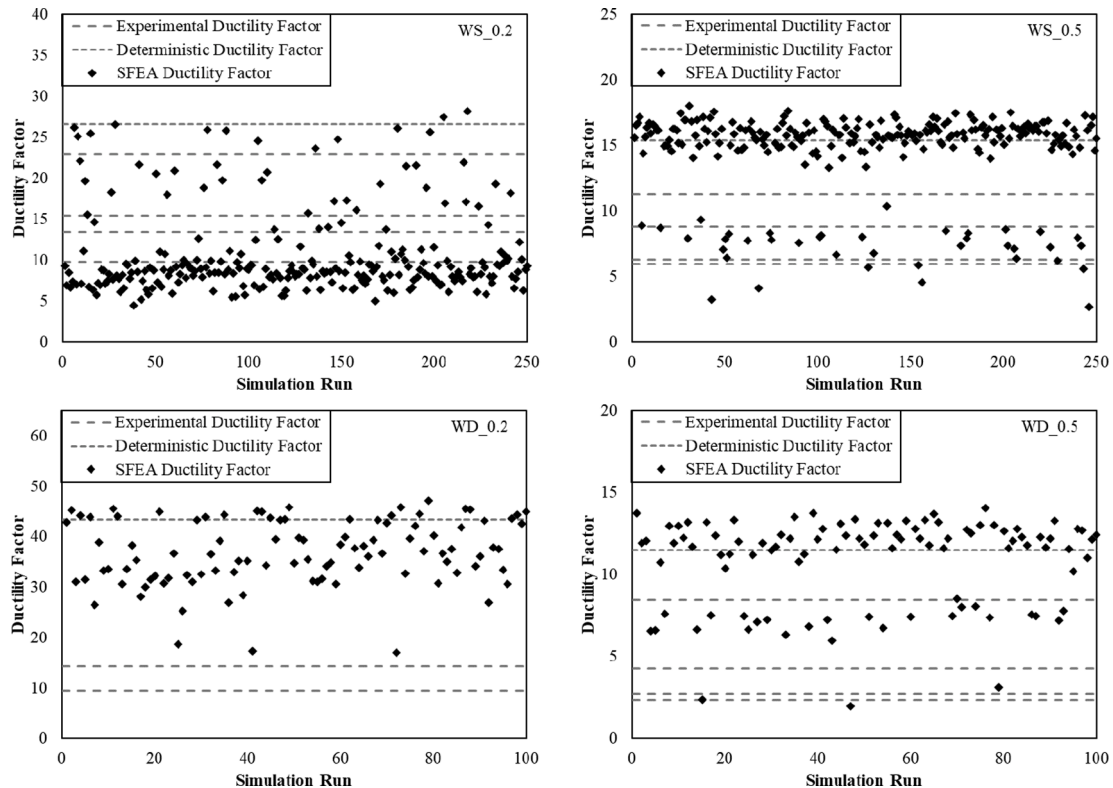


Fig. 21. Ductility factors estimated from SFEAs, utilising the bilinearisation method presented by Magenes et al., [21].

This is due to the sharp post-peak drop off of load resistance observed in the majority of Monte-Carlo simulations of this wall configuration.

A discrepancy, similar to that of the mean and deterministic strength estimated of WD_0.5 discussed previously, is noted between the mean value of ductility estimated from the SFEAs and the deterministic models in two of the scattergrams presented in Fig. 21. In this case, this distinction is due largely to the limitations of these estimates of ductility discussed above. Furthermore, the presence of weaker than average joints is likely to induce greater post-peak softening as stresses are forced to redistribute, leading to the deterministic models' overestimation of the mean ductility factor.

An improved estimation of the ductility of URM walls may be made utilising the proposed modelling strategy if a stiffness calibration of the structures were to be carried out prior to any Monte-Carlo simulations. This calibration may take the form of a reduced elastic normal and shear stiffness of the masonry continuum elements, as well as that of the non-linear interface elements. This reduction could be based upon a known or approximated relationship of the elastic stiffness of an experimental test and an equivalent FE model.

5.4. Sensitivity analysis of spatial variability

A key component of the work undertaken in this study is the consideration of the influence spatial variability of material properties within the examined shear walls. The effect of spatial variability was examined by comparing the results discussed above with those obtained from nonspatial SFEAs. The latter involved multiple simulations using randomly generated material inputs, but in each simulation, material properties are uniform across the height and length of the wall (i.e. fully correlated; $\rho = 1$). It was found that consideration of spatial variability of material properties within each wall simulation did not greatly affect the estimated mean peak resistance, compared to the nonspatial simulations. However, it did have a significant effect on the variability, decreasing greatly the COV of peak wall resistance in some cases, as shown in Table 6. This observation can be explained by the fact that when failure initiates at a weaker than average joint or unit within the wall, the presence of stronger surrounding material in a spatially variable simulation allows for more effective stress redistribution (load sharing) compared to a nonspatial model in which all the surrounding material has the same strength. This averaging effect which occurs in a spatially variable system results in much lower variability in the system response. The slightly lower mean peak wall strength observed in three of the four cases investigated can be attributed to the higher probability of encountering a weak joint or unit in each spatial simulation, compared to the nonspatial simulations. A similar trend of high COVs of wall strength for nonspatial SFEAs, was observed for URM walls subjected to out-of-plane bending by Li et al., [17].

Table 6
Effect of spatial variability on peak in-plane shear resistance.

Wall configuration	Mean			COV	
	Deterministic (kN)	Nonspatial (kN)	Spatial (kN)	Nonspatial	Spatial
WS_0.2	39.5	39.9	39.6 (0.8%)	3.8%	2.0%
WS_0.5	70.8	72.4	71.0 (2.0%)	9.2%	1.2%
WD_0.2	43.4	44.7	45.0 (0.7%)	2.4%	1.9%
WD_0.5	82.2	81.9	80.2 (2.1%)	5.6%	1.4%

* Bracketed values refer to percentage difference between spatial and nonspatial models.

6. Conclusions

An FE modelling strategy was developed for URM walls subjected to in-plane lateral loading. Utilising this approach, the suitability of a monotonic loading scheme in the modelling of a cyclically loaded URM shear wall was examined. It was found that the monotonic approach produced a good fit to the load–displacement envelope of cyclically loaded experimental tests, as well as producing a good and somewhat conservative estimate of the peak load resistance of these walls. The influence of spatial variability of material properties within these URM walls was examined through the application of Monte-Carlo simulations. It was observed that the SFEAs produced a better estimation of the experimental mean strength than any of the deterministic models. While it was also noted that the variability of the peak strength was very low in all cases, the COVs of peak strength were consistent with those obtained from the experimental tests. It may be concluded that this is caused by the observed failure modes in the wall configurations investigated being mostly dependent upon the wall geometries and boundary conditions, more so than on the material strengths. It was observed that in almost all cases, a rocking failure was induced, with initial cracking occurring in one of the first few bed joints of the tensile pier. It is expected that structures that are more susceptible to alternate failure modes; specifically, structures that have a smaller height-to-length ratio or are more highly confined will exhibit a greater variability in their peak strength due to the presence of alternate, and less geometrically constrained failure modes. While the results of this study were found to be limited to a relatively invariable failure mechanism, the procedures and stochastic models presented in this paper may be applied to future SFEAs of URM shear walls.

In addition to the observations made of peak strength estimates, investigation into the ductility and force–displacement response of the deterministic and SFEAs was undertaken. It was found that due to an overestimation of the elastic stiffness of the examined structures, the yield displacement of each simulation was notably smaller than that observed experimentally. Furthermore, this underestimation of the yield displacement resulted in a greater degree of softening to occur within the examined range of in-plane displacements. As a result, estimations of the ductility factors for each structural configuration were inaccurate. It is expected that this inaccuracy could be rectified through the application of a stiffness factor applied to the linear normal and shear stiffness of each FEA.

Finally, a sensitivity analysis of the effect of spatial variability of material properties was performed. This investigation involved the creation and assessment of an additional set of SFEAs, where the variability of material properties was applied non-spatially, i.e.: each stochastically generated material property was considered constant throughout a given simulation. It was observed that the consideration of spatial variability has little effect on the peak shear resistance of each structural configuration but had a notable effect on the estimated COV. Due to the greater load-sharing capacity of a spatially variable model, the COV of spatially variable SFEAs was significantly lower than that of non-spatial models and was more consistent with the results obtained experimentally.

7. Future work

It is recommended that future work includes the examination of structures more susceptible to sliding and diagonal cracking failures so that an understanding of the variability of these failure mechanisms, and how they affect the global failure uncertainty may be established. Furthermore, it is recommended that URM shear walls of a regular geometry are examined so that existing analytical models of in-plane shear strength may be more readily applied. This will allow for the application of simplified Monte-Carlo simulations, based upon the determined stochastic material models, to be used in conjunction with the methods applied in this study.

CRedit authorship contribution statement

Lewis J. Gooch: Conceptualization, Methodology, Software, Validation, Formal analysis, Investigation, Writing - original draft, Writing - review & editing, Visualization. **Mark J. Masia:** Methodology, Resources, Conceptualization, Validation, Writing - review & editing, Supervision, Project administration, Funding acquisition. **Mark G. Stewart:** Methodology, Resources, Conceptualization, Validation, Writing - review & editing, Supervision, Project administration, Funding acquisition.

Declaration of Competing Interest

The authors declare that they have no known competing financial interests or personal relationships that could have appeared to influence the work reported in this paper.

Acknowledgements

The support and resources provided by Dr. Howlader are appreciated. The financial support provided by the Australian Research Council Discovery Project DP180102334 is gratefully acknowledged.

References

- [1] ASTM International. Standard Test Methods for Cyclic (Reversed) Load Test for Shear Resistance of Vertical Elements of the Lateral Force Resisting Systems for Buildings. West Conshohocken: ASTM International; 2011.
- [2] Betti M, Galano L, Vignoli A. Comparative analysis on the seismic behaviour of unreinforced masonry buildings with flexible diaphragms. *Eng Struct* 2014;61:195–208.
- [3] DIANA FEA, 2019. DIANA 10.3 - User's Manual, Delft: s.n.
- [4] Drysdale RG, Hamid AA, Baker LR. *Masonry Structures: Behaviour and Design*. New Jersey: Prentice-Hall; 1994.
- [5] Ellingwood, B., Galambos, T. V., MacGregor, J. G. & Cornell, C. A., 1980. Development of a Probability Based Load Criterion for American National Standard A58. Special Publication 577 ed. Washington D.C.: National Bureau of Standards.
- [6] Ellingwood BR. Analysis of Reliability of Masonry Structures. *Journal of Structural Division* 1981;197(ST5):756–73.
- [7] Ellingwood BR, Tallin A. Limit States Criteria for Masonry Construction. *J Struct Eng* 1985;111(1):108–22.
- [8] European Standard, 2002. Methods of test for masonry. Design code EN1052-3. Brussels: European committee of standardization.
- [9] Farshci DM, Motavalli M, Schumacher A, Marefat MS. Numerical modelling of in-plane behaviour of URM walls and an investigation into the aspect ratio, vertical and horizontal post-tensioning and head joint as a parametric study. *Archives of Civil and Mechanical Engineering* 2009;9(1):5–27.
- [10] Fenton GA. Estimation for Stochastic Soil Models. *J Geotech Geoenviron Eng* 1999;470–85.
- [11] Heffler LM. Variability of Unit Flexural Bond Strength and its Effect on Strength in Clay Brick Unreinforced Masonry Walls Subject to Vertical Bending. Callaghan: University of Newcastle; 2009.
- [12] Heffler LM, Stewart MG, Masia MJ, Correa MRS. Statistical Analysis and Spatial Correlation of Flexural Bond Strength for Masonry. *Masonry International* 2008;21(2):59–70.
- [13] Howlader MK, Masia MJ, Griffith MC. Numerical analysis and parametric study of unreinforced masonry walls with arch openings under lateral in-plane loading. *Eng Struct* 2020;208.
- [14] Lawrence, S. J., 2009. Size effect in vertically spanning unreinforced masonry walls [Paper C1-4]. Toronto, Ontario, Canada, Proc. 11th Canadian Masonry Symposium.
- [15] Li J. *Spatial Variability and Stochastic Strength Prediction of Unreinforced Masonry Walls Subjected to Out-of-Plane Bending*. Callaghan: University of Newcastle; 2015.
- [16] Li J, Masia MJ, Stewart MG. Stochastic spatial modelling of material properties and structural strength of unreinforced masonry in two-way bending. *Struct Infrastruct Eng* 2017;13(6):683–95.
- [17] Li J, Stewart MG, Masia MJ, Lawrence SJ. Spatial Correlation of Material Properties and Structural Strength of Masonry in Horizontal Bending. *J Struct Eng* 2016;142(11).
- [18] Lourenço PB. *A user/programmer guide for the micro-modelling of masonry structures*. Delft: Delft University of Technology; 1996.
- [19] Lourenço PB. *Computational Strategies for Masonry Structures*. Delft: Delft University of Technology; 1996.
- [20] Lourenço PB, Rots JG. *Multisurface Interface Model for Analysis of Masonry Structures*. *J Eng Mech* 1997;123(7):660–8.
- [21] Magenes G, Morandi P, Penna A. Test results on the behaviour of masonry under static cyclic in plane lateral loads. Pavia: Department of Structural Mechanics, University of Pavia; 2008.
- [22] Malyszko L. In-plane shear and tensile strength tests of small brickwork specimens. In: Modena C, Lourenço PB, Roca P, editors. *Structural Analysis of Historical Constructions: Possibilities of Numerical and Experimental Techniques*. London: A. A. Balkema Publishers; 2004. p. 291–8.
- [23] Masia MJ, et al. Torsion shear test for mortar joints in masonry: preliminary experimental results. s.n.: St. Louis; 2007. p. 968–79.
- [24] Mojsilović N, Stewart MG. Probability and structural reliability assessment of mortar joint thickness in load-bearing masonry walls. *Struct Saf* 2015;52:209–18.
- [25] Müller D, Föster V, Graubner C-A. Influence of material spatial variability on required safety factors for masonry walls in compression. *Mauerwerk* 2017;21(4):209–22.
- [26] Petersen RB. *In-plane Shear Behaviour of Unreinforced Masonry Panels Strengthened with Fibre Reinforced Polymer Strips*. Callaghan: University of Newcastle; 2009.
- [27] Peterson RB, Ismail N, Masia MJ, Ingham JM. Finite element modelling of unreinforced masonry shear walldettes strengthened using twisted steel bars. *Constr Build Mater* 2012;33:14–24.
- [28] Priestley M. *Spectral Analysis and Time Series*. London: Academic Press; 1981.
- [29] Raphael JM. Tensile Strength of Concrete. *ACI Journal* 1984;81(2):158–65.
- [30] Schmidt U, Hannawald J, Brameshuber W. *Theoretical and practical research on the flexural strength of masonry*. Sydney, Proc. 14th International Brick and Block Masonry Conference. 2008.
- [31] Standards Australia, Standards New Zealand, 2003. *Masonry units, segmental pavers and flags - Methods of test. Method 15: Determining lateral modulus of rupture*. Sydney: Standards Australia, Standards New Zealand.
- [32] Australia S. *Steel Structures*. Sydney: Standards Australia; 1998.
- [33] Australia S. *Concrete Structures*. Sydney: Standards Australia; 2018.
- [34] Australia S. *Masonry structures*. Sydney: Standards Australia; 2018.
- [35] Stewart MG, Lawrence SJ. *Structural Reliability of Masonry Walls in Flexure*. *Masonry International* 2002;15(2):48–52.
- [36] Stewart MG, Lawrence SJ. Model Error, Structural Reliability and Partial Safety Factors for Structural Masonry in Compression. *Masonry International* 2007;20(3):107–16.
- [37] Stewart MG, Lawrence SJ. Model Error and Structural Reliability for Unreinforced Masonry Walls in Vertical Bending. *Masonry International* 2011;24(1):23–30.
- [38] Turkstra CJ. *Limit States Design in Masonry*. San Francisco, Proc. In: 5th International Conference on Structural Safety and Reliability; 1989. p. 2043–50.
- [39] Van der Pluijm R. Non-linear Behaviour of Masonry under Tension. *Heron* 1997;42(1):25–54.
- [40] Zhang S, et al. Numerical modelling of FRP-reinforced masonry walls under in-plane seismic loading. *Constr Build Mater* 2017;134:649–63.